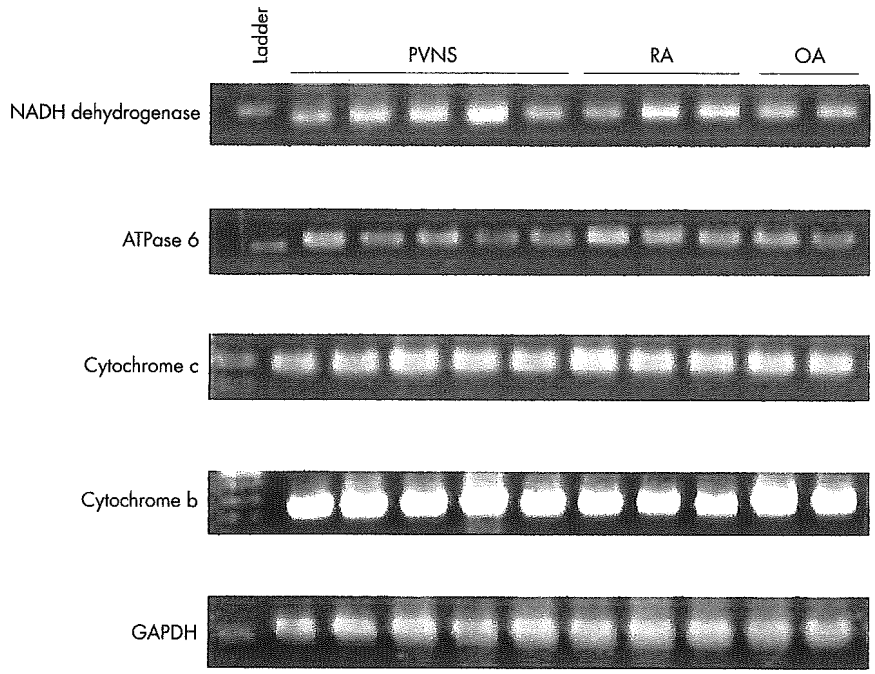

Figure 3 The expression of genes encoded in mitochondria other than humanin genes. Total RNA was extracted from the synovial cells of five patients with PVNS, three with RA, and three with OA, and NADH dehydrogenase, ATPase 6, cytochrome *c*, cytochrome *b*, and GAPDH mRNA levels were analysed by semiquantitative RT-PCR. The levels of expression of these genes in PVNS were not increased in other types of arthritis, indicating that the humanin gene was selectively expressed in mitochondrial genes in PVNS.

a PAG mini Daiichi 15/25 gel (Daiichi Pure Chemical Co). The gel electrophoresis was performed under non-reducing conditions. The proteins were then blotted onto a nitrocellulose blotting membrane (Osmonics Inc). Nitrocellulose membranes were blocked with 5% BSA, followed by washing with PBS-Tween 20, and incubated with rabbit anti-humanin antibody at 4℃ overnight. After intensive washing, membranes were incubated with horseradish peroxidase linked goat antirabbit IgG, followed by detection with enhanced chemiluminescence reagents (Biotechs).

Electron microscope and colloidal gold immunocytochemistry

Synovial cells from diffuse-type PVNS were gathered in the same manner for light microscopy, and fixed in 3% glutaraldehyde in 0.1 M phosphate buffer (pH 7.4) at 4℃ over night. The specimens were postfixed in 1% OsO_4 in 0.1 M phosphate buffer (pH 7.4) overnight at 4℃, rinsed three times (10 minutes each) in 10% saccharose, and stained all together in 3% aqueous uranyl acetate for 1 hour at room temperature. Samples were then dehydrated in an ascending series of ethanol concentrations, replaced by propylene oxide, and embedded in epoxy resin. Ultrathin sections (100 nm) were cut, stained with uranyl acetate and lead citrate, and observed using an electron microscope (Hitachi H-7000).

For electron microscopic immunocytochemistry, cells were fixed in 0.2% glutaraldehyde and 4% paraformaldehyde mixture in 0.1 M phosphate buffer (pH 7.4) at 4℃ overnight. The samples were embedded into Lowicryl K4M, and ultrathin sections (100 nm) were used for incubation with anti-humanin antibody overnight. Incubation with the biotinylated secondary antibody was performed at room temperature for 1 hour, and after washing with PBS and distilled water, incubation with colloidal gold streptavidin was performed for 1 hour. The sections were rinsed and dried, then stained with uranyl acetate and lead citrate, and electron microscopy was performed as described above.

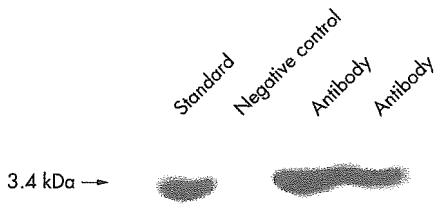

Figure 4 Expression of humanin peptide in synovial cells from diffuse-type PVNS. Protein (20 μg) from synovial cell lysates was subjected to SDS-PAGE on a 5–20% gradient gel. Rabbit anti-humanin polyclonal antibody was used for western blotting. Synthesised peptide, which was used as antigen to produce rabbit anti-humanin polyclonal antibody, was used as a standard and rabbit IgG was used as a negative control.

RESULTS

Identification of highly expressed genes in PVNS

A total of 2956 clones selected by subtraction cloning were further examined by Southern colony hybridisation. The sequencing was performed on genes expressed in PVNS at three times greater frequency than those in RA. Sixty eight of the highly expressed genes were identical to 17 known genes. Two genes were identical to genes encoding two hypothetical proteins. Table 1 classifies these genes into seven groups according to their functions and whether they were transcribed in mitochondria. Interestingly, genes encoded in the region of 16S rRNA and 12S rRNA were expressed with high frequencies. Furthermore, we detected various forms of 16S rRNA with poly A tail end, as shown in fig 1. No 12S rRNA with poly A tail was found among these genes. The cDNA with poly A tail (16S rRNA•3229: type 9 in fig 1) was identical to the humanin gene.

Northern blot analysis was performed using mRNA of synovial cells from patients with PVNS, RA, and OA. Humanin genes were strongly expressed in diffuse-type PVNS, but were barely detectable in nodular-type PVNS, RA, or OA (fig 2). However, other genes encoded by mitochondria were not increased as assessed by semiquantitative RT-PCR, suggesting

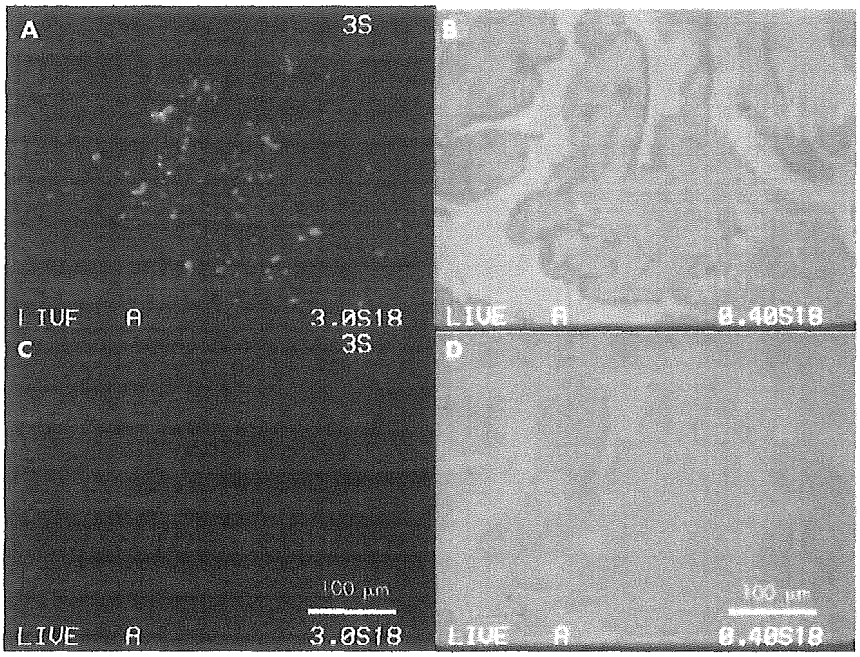

Figure 5 Synovial tissue from diffuse-type PVNS was fixed with 4% formaldehyde in PBS. The specimens were stained with anti-humanin antibody, followed by Alexa 488 goat antirabbit IgG, and photographed with a fluorescent microscope (×40). (A) Most positive cells (green) were distributed in a deep layer with haemosiderin deposit. (C) Negative control of the continuous section. (B, D) Backgrounds for (A) or (C), respectively.

that ribosomal genes were selectively expressed in mitochondrial genes in PVNS (fig 3). As far as we know, this is the first report of the expression of the humanin gene in synovial cells.

Expression of the humanin peptide in PVNS

Next, the expression of humanin peptide was identified using synovial cell lysates from diffuse-type PVNS and anti-humanin polyclonal antibody (fig 4). Immunohistochemical analysis showed that most of the positive cells were distributed in the deep layer (fig 5). This positive staining was thoroughly suppressed by blocking the primary antibody with synthesised antigen peptide (data not shown).

Although it has been suggested that the humanin peptide is expressed by cells in the deep layer of PVNS, little is known about the intracellular localisation of this peptide. In further examinations, we detected intracellular humanin peptide in synovial cells from diffuse-type PVNS. The humanin peptide was stained with a red colour, which localised in the cytoplasm of the synovial cells (fig 6B) but not in the nucleus. Mitochondria were stained with a green colour using anti-hsp60, which is mitochondrial-specific chaperonin (fig 6C). Double staining with anti-humanin antibody and anti-hsp60 (yellow colour) demonstrated that humanin was expressed mainly in the mitochondria (fig 6D).

Electron microscopic observation of synovial cells from diffuse-type PVNS showed that most of the iron deposits were included within the siderosome as described previously.[16 17] However, some electron dense iron deposits were

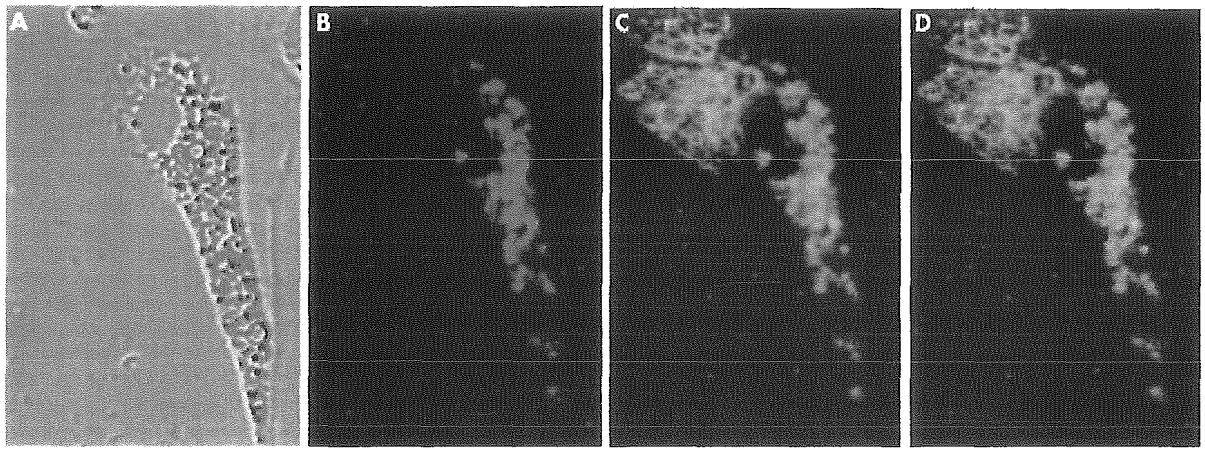

Figure 6 Relationship between humanin peptide expression and mitochondria. Isolated synovial cells containing haemosiderin were double stained with anti-humanin antibody and anti hsp60 antibody as first antibodies, followed by goat antirabbit IgG and donkey antigoat IgG as second antibodies (×400). (A) Haemosiderin was deposited unequally throughout the cytoplasm. (B) Single anti-humanin antibody staining (red). (C) Single anti-hsp60 antibody staining (mitochondrial staining; green). (D) Humanin was dominantly distributed in the mitochondria around the siderosome (yellow).

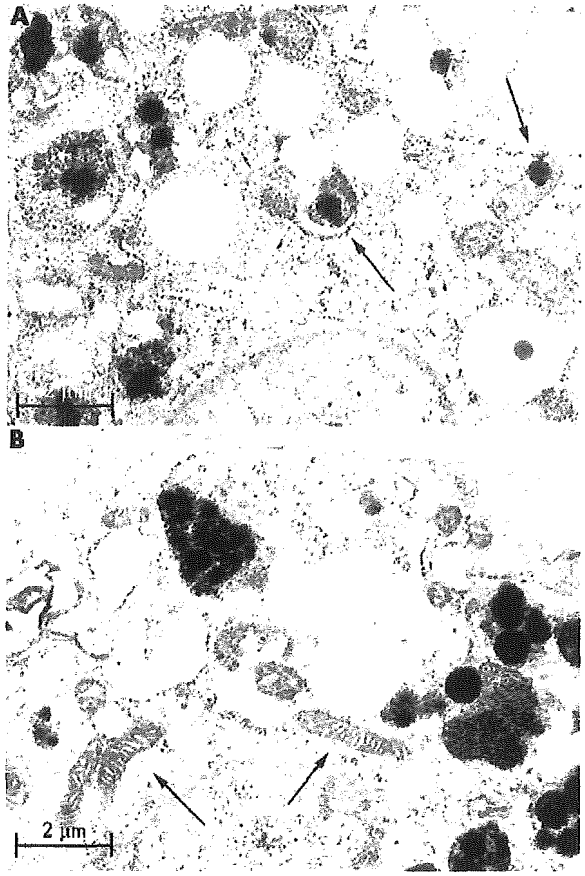

Figure 7 Electron micrograph of synovial cells from diffuse-type PVNS. Most of the electron dense iron deposits were observed within the siderosomes. Some electron dense iron deposits were observed within mitochondria (arrows). (A) Mitochondrial membrane debris with electron dense deposits was observed within the siderosome as an autophagosome (left arrow). (B) Some of the normal mitochondria (arrows) also were scattered throughout the cytoplasm. (Magnification ×19 000.)

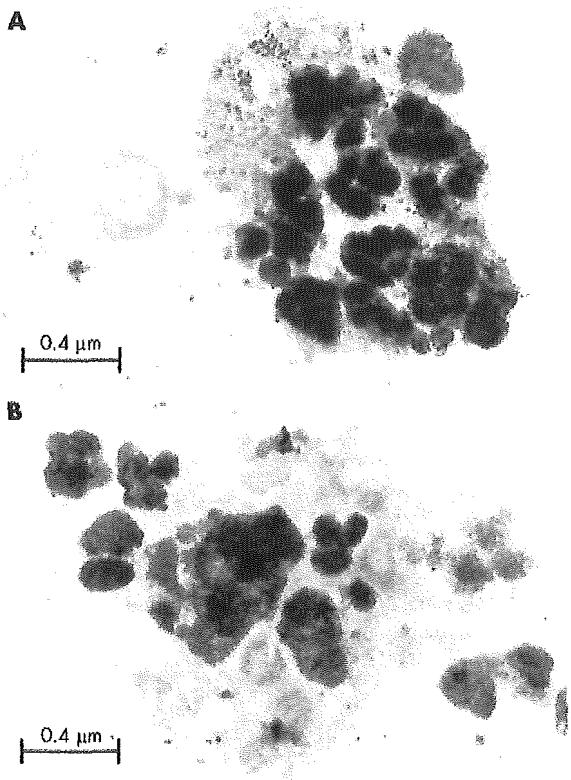

Figure 8 Electron microscopic immunohistochemistry of synovial cells from diffuse-type PVNS. (A) In some of the siderosomes, particles of colloidal gold, were precipitated in the debris adjacent to electron dense iron. These results demonstrate that humanin peptide is present within the debris that is phagocytosed into the siderosome. (B) Negative control for immunohistochemistry. (Magnification ×29 000.)

observed within the mitochondria (fig 7A). Interestingly, mitochondrial membrane debris with electron dense iron deposits were observed within the siderosome, which was characterised as an autophagosome (fig 7A). On the other hand, some normal mitochondria were scattered throughout the cytoplasm (fig 7B). Electron dense iron deposits within the siderosome were observed by electron microscopic immunohistochemistry (fig 8). In some siderosomes, particles of colloidal gold were precipitated in the debris adjacent to electron dense iron (fig 8A). These results suggest that humanin exists in mitochondria not only in the cytoplasm but also in the siderosome after being phagocytosed.

DISCUSSION

Genes with enhanced expression in synovial cells from PVNS were grouped according to their functions and the transcription in mitochondria as listed in table 1. It is likely that many of the listed genes play a part in the pathogenesis of PVNS according to their characterised functions. Interestingly, genes encoded in the regions of 16S rRNA and 12S rRNA were expressed with high frequencies. Previous reports pointed out the presence of polyadenylated transcripts of the 16S rRNA gene that differed from the 16S rRNA.[24–26] These poly A sequences are considered to be due to active metabolism of mitochondria in cancer cells, because the increased expression of the 16S rRNA genes was found only in malignancies.[19 27] These facts suggest that the genes encoded in the region of rRNA from PVNS reflect the neoplastic nature of this disease. In fact, for PVNS, especially the diffuse type, the neoplastic hypothesis is supported by the demonstration of aneuploid DNA content and the existence of cytogenetic aberration, as well as the capacity of these lesions for autonomous growth and the potential for recurrence.[13 14]

It is intriguing to examine whether these mitochondrial genes for 16S rRNA are virtually translated and act as functional peptides. In this regard, humanin is a polypeptide described as a rescue factor abolishing neural cell apoptosis. This peptide protects neural cells of the F11 line from death induced by the expression of mutated genes, causing early onset familiar Alzheimer's disease.[28] Additionally, it was reported that humanin protects CN-procaspase-3 from amyloid precursor protein-induced cleavage, thereby preventing apoptosis.[29–31] More recently, Guo *et al* also described the anti-apoptotic mechanism of this peptide through interference with Bax activation.[20] In this study we proved that the humanin peptide, encoded in the mitochondrial genome, was selectively expressed in the mitochondria and within the siderosome in the diffuse-type PVNS synovial cells. It is well established that damaged and functionally disabled mitochondria may be autophagocytosed by lysosomes to prevent continuous oxidative damage, as shown in the degenerating mitochondria within the siderosome in our electron microscopic study.[32 33] This evidence suggests that humanin is translated in mitochondria, leading to survival of

this organelle under the condition of excessive iron deposition.

In fact, extreme iron deposition is one of the most characteristic pathological features in PVNS.[2 7 8] This deposit is derived from the breakdown of erythrocytes that are phagocytosed after repeated bleeding into the joint space.[16 34 35] Under the condition of iron excess, some of the iron is shunted into haemosiderin and stored in the cytoplasm.[36] It is well described that reactive oxygen species are generated by excessive iron-induced cell apoptosis, which is one important mechanism implicated in the mitochondrial death pathway.[36–40] This mechanism may involve the capacity of excessive iron deposits to stimulate lipid peroxidation, thereby disrupting lysosomal membranes and releasing tissue destructive hydrolytic enzymes.[41 42] In regard to PVNS, as shown in our subtraction cloning, the iron deposits are known to be associated with large quantities of ferritin. Nevertheless, homogeneous synovial cells with small, rounded siderosomes in the deep layer of synovium, which present predominantly in diffuse-type PVNS, were reported to have minimum tissue damage adjacent to the iron deposits.[43] Morris *et al* reported that electron dense iron deposits were associated with mitochondrial destruction in haemophilic synovitis but much less so in PVNS.[43] Several explanations were suggested for this lack of mitochondrial damage in previous reports, such as transitional function during inflammation, or the failure of the apoferritin response.[31 43] However, there were no facts to explain this pathology.

The alternative intriguing explanation about this pathogenesis of PVNS is that a mitochondrial abnormality exists primarily in PVNS which is independent of the precipitation of haemosiderin. In that case, the overload of iron deposits in the cytoplasm and mitochondria could induce free radicals. However, abnormal mitochondria would be responsible for supplying a key reactant, humanin, to prevent oxidative damage until they are autophagocytosed within the siderosome, resulting in cell survival. In accordance with this view, analysis of isolated cells has enabled us to describe here for the first time the feature of mitochondria containing haemosiderin, which were autophagocytosed and degenerating within the siderosome, in addition to many mitochondria without haemosiderin scattered around the cytoplasm.

Taken together, our findings lead us to a simple interpretation that the possible function of humanin located within the mitochondria in PVNS synovial cells may be to serve as a rescue factor from excessive iron damage and consequent organelle breakdown in the cytoplasm and cell death. However, Hashimoto *et al* have shown that cell death is only supported by the secreted humanin peptide,[29] and the function of the peptide located intracellularly is still unclear. Although future studies are required to investigate the function of humanin within the cytoplasm, our data suggest that humanin is involved in the iron depositing pathology of PVNS. In conclusion, our results suggest that the humanin peptide is highly expressed in the synovial cells from diffuse-type PVNS and may play a part in the pathology of PVNS.

ACKNOWLEDGEMENTS

We thank A Tsuchiya MD and S Tsuyama MD for their professional advice.

Authors' affiliations
K Ijiri, H Sakakima, Course of Physiotherapy, School of Health Science, Faculty of Medicine, Kagoshima University, Kagoshima, Japan
K Ijiri, M B Goldring, Beth Israel Deaconess Medical Center, New England Baptist Bone and Joint Institute, Boston, MA, USA
H Tsuruga, T Matsuyama, Immunology and Medical Zoology, Graduate School of Medicine, Kagoshima University, Kagoshima, Japan
N Taniguchi, K Shimoonoda, S Komiya, Department of Neuro-Musculoskeletal Disorder, Kagoshima University Graduate School of Medicine and Dentistry, Kagoshima University, Kagoshima, Japan
K Tomita, H J Majima, Department of Oncology, Kagoshima University Graduate School of Medicine and Dental Science, Kagoshima, Japan

REFERENCES

1 **Jaffe HL**, Lichtenstein L, Sutro CJ. Pigmented villonodular synivitis, bursitis and tenosynovitis. *Arch Pathol* 1941;**31**:731–65.
2 **Dorwart RH**, Genant HK, Johnston WH, Morris JM. Pigmented villonodular synovitis of synovial joints: clinical, pathologic, and radiologic features. *AJR Am J Roentgenol* 1984;**143**:877–85.
3 **Darling JM**, Glimcher LH, Shortkroff S, Albano B, Gravallese EM. Expression of metalloproteinases in pigmented villonodular synovitis. *Hum Pathol* 1994;**25**:825–30.
4 **Gehweiler JA**, Wilson JW. Diffuse biarticular pigmented villonodular synovitis. *Radiology* 1969;**93**:845–51.
5 **Crosby EM**, Inglis A, Bullough PG. Mulitple joint involvement with pigmented villonodular synovitis. *Radiology* 1977;**122**:671–2.
6 **Wagner ML**, Spjut HJ, Dutton RV, Glassman AL, Askew JB. Polyarticular pigmented villonudular synovitis. *AJR Am J Roentgenol* 1981;**136**:821–3.
7 **Byers PD**, Cotton RE, Deacon OW, Lowy M, Newman PH, Sissons HA, *et al*. The diagnosis and treatment of pigmented villonodular synovitis. *J Bone Joint Surg Br* 1968;**50**:290–305.
8 **Jozsa L**. Immunohistochemical characterization of pigmented villonodular synovitis. *Zentralbl Pathol* 1992;**138**:119–23.
9 **O'Connell JX**, Fanburg JC, Rosenberg AE. Giant cell tumor of tendon sheath and pigmented villonodular synovitis. Immunophenotype suggests a synovial cell origin. *Hum Pathol* 1995;**26**:771–5.
10 **Darling JM**, Goldring SR, Harada Y, Handel ML, Glowacki J, Gravallese EM. Multinuclear cells in pigmented villonodular synovitis and and giant cell tumor of tendon sheath express features of osteoclasts. *Am J Pathol* 1997;**150**:1383–92.
11 **Young JM**, Hudacek AG. Experimental production of pigmented villonodular synovitis in dogs. *Am J Pathol* 1954;**30**:799–811.
12 **Sigh R**, Grewal DS, Chakravarti RN. Experimental production of pigmented villonodular synovitis in the knee and ankle joints of rhesus monkey. *J Pathol* 1969;**98**:137–42.
13 **Somerhausen NSA**, Fletcher CDM. Diffuse-type giant cell tumor. Clinicopathologic and immunohistochemical analysis of 50 cases with extraarticular disease. *Am J Surg Pathol* 2000;**24**:479–92.
14 **Abdul-Karim FW**, El-Naggar AK, Joyce MJ, Makley JT, Carter JR. Diffuse and localized tenosynovial giant tumor and pigmented villonodular synovitis: a clinicopathological and flow cytometric DNA analysis. *Hum Pathol* 1992;**23**:729–35.
15 **Fletcher JA**, Henkle C, Atkins L, Rosenberg AE, Morton C. Trisomy 5 and trisomy 7 are nonrandom aberrations in pigmented villonodular synovitis: confirmation of trisomy 7 in uncultured cells. *Genes Chromosomes cancer* 1992;**4**:264–6.
16 **Schumacher HR**, Lotke P, Athreya B, Rothfuss S. Pigmented villonodular synovitis: light and electron microscopic studies. *Semin Arthritis Rheum* 1982;**12**:32–43.
17 **Ghadially FN**, Lalonde J-M A, Dick CE. Ultrastructure of pigmented villonodular synovitis. *J Pathol* 1978;**127**:19–27.
18 **Wyllie JC**. Stromal cell reaction of pigmented villonodular synovitis: an electron microscopic study. *Arthritis Rheum* 1969;**12**:205–14.
19 **Maximov V**, Martynenko A, Hunsmann G, Tarantul V. Mitochondrial 16S rRNA gene encodes a functional peptide, a potential drug for Alzheimer's disease and target for cancer therapy. *Med Hypotheses* 2002;**59**:670–3.
20 **Guo B**, Zhai D, Cabezas E, Welsh K, Nlourain S, Tatterthwait A, *et al*. Humanin peptide suppresses apoptosis by interfering with Bax activation. *Nature*. 2003;423: 456–61, Epub 4 May, 2003.
21 **Chomczynski P**, Sacchi N. Single-step method of RNA isolation by acid guanidinium thiocyanate-phenol-chlorform extraction. *Anal Biochem* 1987;**162**:156–9.
22 **Majima JH**, Oberley TD, Fukukawa K, Mattson MP, Yen HC, Szweda LI, *et al*. Prevention of mitochondrial injury by manganese superoxide dismutase reveals a primary mechanism for alkaline-induced cell death. *J Biol Chem* 1998;**273**:8217–24.
23 **Motoori S**, Majima HJ, Ebara M, Kato H, Hirai F, Kakinuma S, *et al*. Overexpression of mitochondrial manganese superoxide dismutase protects against radiation-induced cell death in the human hepatocellular carcinoma cell line, HLE. *Cancer Res* 2001;**61**:5382–8.
24 **Peng G**, Taylor JD, Tchen TT. Increased mitochondrial activites in pigmented (melanized) fish cells and nucleotide sequence of mitochondrial large rRNA. *Biochem Biophys Res Commun* 1992;**189**:445–9.
25 **Baserga SJ**, Linnenbach AJ, Malcolm S. Polyadenylation of a human mitochondrial ribosomal RNA transcript detected by molecular cloning. *Gene* 1985;**35**:305–12.
26 **Tarantul V**, Nikolaev A, Hannig H. Detection of abundantly transcribed genes and gene translocation in human immunodeficiency virus-associated non-Hodgkin's lymphoma. *Neoplasia* 2001;**3**:132–42.
27 **Penta J**, Johnson FM, Wachsman JT, Copeland WC. Mitochondrial DNA in human malignancy. *Mutat Res* 2001;**488**:119–33.
28 **Hashimoto Y**, Niikura T, Tajima H, Yasukawa T, Sudo H, Ito Y, *et al*. A rescue factor abolishing neural cell death by a wide spectrum of familial Alzheimer's disease. *Proc Natl Acad Sci USA* 2001;**98**:6336–41.

29 **Hashimoto Y**, Ito Y, Niikura T. Mechanism of neuroprotection by a novel rescue factor humanin from Swedish mutant amyloid precursor protein. *Biochem Biophy Res Commun* 2001;**283**:460–8.
30 **Yu W**, Sanders BG, Kline K. RRR-alpha-tocopheryl succinate-induced apoptosis of human breast cancer cells involved bax translocation to mitochondria. *Cancer Res* 2003;**63**:2483–91.
31 **Nakazawa Y**, Kamijo T, Koike K, Noda T. ARF tumor suppressor induces mitochondria-dependent apoptosis by modulation of mitochondrial Bcl-2 family proteins. *J Biol Chem*. 2003;278: 27888–95, Epub 9 May, 2003.
32 **Muirden KD**. The anemia of rheumatoid arthritis: the significance of iron deposits in the synovial membrane. *Aust Ann Med* 1970;**2**:97–104.
33 **Brunk UT**, Terman A. The mitochondrial-lysosomal axis theory of aging: accumulation of damaged mitochondria as a result of imperfect autophagocytosis. *Eur J Biochem* 2002;**269**:1996–2002.
34 **Morris CJ**, Wainwright AC, Steven MM. The nature of iron deposits in haemophilic synovitis – an immunohistochemical ultrastructural and x-ray microanalytical study. *Virchows Arch A Pathol Anat Histopathol* 1984;**404**:75–85.
35 **Docken WP**. Pigmented villonodular synovitis: a review with illustrative case reports. *Semin Arthritis Rheum* 1979;**9**:1–22.
36 **Wixom RL**, Prutkin L, Munro HN. Hemosiderin: nature, formation, and significance. *Intl Rev Exp Pathol* 1980;**22**:193–225.
37 **Chamberlain MA**, Petts V, Gallins E. Transport of intravenously injected ferritin across the guinea-pig synovium. *Ann Rheum Dis* 1972;**31**:493–9.
38 **McCord JM**, Roy RS. The pathophysiology of superoxide; roles in inflammation and ischaemia. *Can J Physiol Pharmacol* 1982;**60**:1346–52.
39 **Halliwell B**, Gutteridge JM. Oxygen toxicity, oxygen radicals, transition metals and disease. *Biochem J* 1984;**219**:1–4.
40 **Panduri V**, Weitzman SA, Chandel N, Kamp DW. The mitochondria-regulated death pathway mediates asbestos-induced alveolar epithelial cell apoptosis. *Am J Respir Cell Mol Biol* 2003;**28**:241–8.
41 **Gutteridge JM**, Halliwell B, Treffry A, Harrison PM, Blake DR. Effect of ferritin containing fractions with different iron loading on lipid peroxidation. *Biochem J* 1983;**209**:557–60.
42 **Crichton RR**. Interreaction between iron metabolism and oxygen activation. In: *Oxygen free radicals and tissue damage*. Amsterdam: Excerpta Medica, 1979:57–76.
43 **Morris CJ**, Blake DR, Wainwright AC, Steven MM. Relationship between iron deposits and tissue damage in the synovium: an ultrastructural study. *Ann Rheum Dis* 1986;**45**:21–6.

ANTIOXIDANTS & REDOX SIGNALING
Volume 6, Number 3, 2004

Forum Original Research Communication

Mitochondrial Signal Lacking Manganese Superoxide Dismutase Failed to Prevent Cell Death by Reoxygenation Following Hypoxia in a Human Pancreatic Cancer Cell Line, KP4

FUTOSHI HIRAI,[1,2] SHIGEATSU MOTOORI,[1] SHIZUKO KAKINUMA,[2] KAZUO TOMITA,[2,3] HIROKO P. INDO,[3] HIROTOSHI KATO,[2] TAKETO YAMAGUCHI,[1] HSIU-CHUAN YEN,[4] DARET K. ST. CLAIR,[5] TETSUO NAGANO,[6] TOSHIHIKO OZAWA,[2] HIROMITSU SAISHO,[1] and HIDEYUKI J. MAJIMA,[2,3,7]

ABSTRACT

One of the major characteristics of tumor is the presence of a hypoxic cell population, which is caused by abnormal distribution of blood vessels. Manganese superoxide dismutase (MnSOD) is a nuclear-encoded mitochondrial enzyme, which scavenges superoxide generated from the electron-transport chain in mitochondria. We examined whether MnSOD protects against hypoxia/reoxygenation (H/R)-induced oxidative stress using a human pancreas carcinoma-originated cell line, KP4. We also examined whether MnSOD is necessarily present in mitochondria to have a function. Normal human MnSOD and MnSOD without a mitochondrial targeting signal were transfected to KP4 cells, and reactive oxygen species, nitric oxide, lipid peroxidation, and apoptosis were examined as a function of time in air following 1 day of hypoxia as a H/R model. Our results showed H/R caused no increase in nitric oxide, but resulted in increases in reactive oxygen species, 4-hydroxy-2-nonenal protein adducts, and apoptosis. Authentic MnSOD protected against these processes and cell death, but MnSOD lacking a mitochondrial targeting signal could not. These results suggest that only when MnSOD is located in mitochondria is it efficient in protecting against cellular injuries by H/R, and they also indicate that mitochondria are primary sites of H/R-induced cellular oxidative injuries. *Antioxid. Redox Signal.* 6, 523–535.

INTRODUCTION

It has been known that hypoxic cells exist in tumors (7, 39) because of irregular localization of blood vessels. The hypoxic cells are resistant to various anticancer treatment modalities, such as radiation, bleomycin, *cis*-platinum, major chemotherapeutic agents utilized in the treatment of cancer, etc. (for review, see 16), which are all major treatments in cancer therapy. These treatment modalities are known to generate reactive oxygen species (ROS) (4, 30, 49). These modalities are effective in killing tumor cells; one of the mechanisms of tumor killing could be related to ROS

[1]First Department of Medicine, Chiba University, School of Medicine, Chiba 260–0856, Japan.
[2]National Institute of Radiological Sciences, Chiba 260-8555, Japan.
[3]Department of Oncology, Kagoshima University Graduate School of Medical and Dental Sciences, Kagoshima 890-8544, Japan.
[4]School of Medical Technology, Chang Gung University, Kwei-Shan, Tao-Yuan 333, Taiwan.
[5]Graduate Center for Toxicology, University of Kentucky, Lexington, KY 40536, U.S.A.
[6]Graduate School of Pharmaceutical Sciences, The University of Tokyo, Tokyo 113-0033, Japan.
[7]Department of Space Environmental Medicine, Kagoshima University Graduate School of Medical and Dental Sciences, Kagoshima 890-8544, Japan.

generation. Further, hypoxic cells may be related to the development of metastasis (31). Hypoxic cells often become reoxygenated after a dose of radiation or intermittent opening of blood vessels (6, 42). This phenomenon has been called reoxygenation (42).

Ischemia/reperfusion (I/R) in a normal brain causes oxidative damage to neuronal cells (for review, see 20, 25). Pathologic events caused by transient tissue hypoxia followed by oxygen reperfusion occur in numerous other tissues (for review, see 10). The pathologic changes encountered following reperfusion of an ischemic organ include an immediate generation of ROS, as well as subsequent inflammatory responses, which lead to a second stage of further ROS generation at the sites of damage. ROS generation following I/R has been examined in various experimental systems *in vivo* and *in vitro* (20). The injuries caused by I/R also occur in organ transplantation (10). One method to increase the effectiveness of organ transplantation may depend on methods to prevent oxidative stress. Clinical trials have been performed to determine whether antioxidant substances will prevent hypoxic-induced injury (10, 20). The use of gene therapy to reduce redox-mediated damage following such I/R injuries is also a subject for clinical consideration (10).

Many neuronal diseases, such as Alzheimer's disease, Parkinson's disease, and amyotrophic lateral sclerosis, and other diseases, such as aging, diabetes, premature babies, and cancer, are now believed to result from oxidative stress (12, 24, 43). Involvement of oxidative stress in tumor tissue is a subject of potentially great importance. Reoxygenation following hypoxia in tumor tissue has been implied to result in better prognosis after radiation therapy, although this hypoxia might also cause acceleration of tumor growth. However, how hypoxia/reoxygenation (H/R) affects tumor cell viability, and the subcellular mechanism(s) involved, have not been well elucidated. Possible changes in tumors may result from mitochondrial degeneration, as well as from subsequent ROS generation in cells (10). Several studies have shown that mitochondria produce superoxide, mainly from complex I and III of the electron transport system, which is located in the inner membrane of mitochondria (5, 36). Production of ROS from the electron transport chain may result in oxidative stress in cells, and may result in apoptotic cell death (23–25, 43). Manganese superoxide dismutase (MnSOD) is an essential enzyme, which scavenges superoxide located in mitochondria (44). The biological importance of MnSOD is demonstrated by the following: (a) A lack of the MnSOD gene in *Escherichia coli* and yeast makes them hypersensitive to oxidative stress (8, 11, 41). (b) Homozygous mutant mice lacking MnSOD died within the first 10 days after birth and showed dilated cardiomyopathy, an accumulation of lipid in the liver and skeletal muscle, and metabolic acidosis (21). (3) Mutant mice lacking MnSOD showed degenerative injury of large central nervous system neurons, particularly in the basal ganglia and brainstem, associated with damaged mitochondria. Also, these mice showed progressive motor disturbances characterized by limb weakness, rapid fatigue, and circling behavior (18). (d) Transfection of MnSOD cDNA into cultured cells rendered the cells resistant to paraquat- (32), tumor necrosis factor- (13, 47), doxorubicin- (13), mitomycin C- (13), radiation- (13, 27, 35), alkaline- (23), and chemical-induced hypoxia (15), cigarette smoke-induced cytotoxicity (34), and radiation-induced neoplastic transformation (33). (e) The expression of human MnSOD genes in transgenic mice protected the mice against oxygen-induced pulmonary injury (45) and adriamycin-induced cardiac toxicity (48). Thus, the expression of MnSOD is essential for the survival of aerobic life and the development of cellular resistance to oxygen radical-mediated toxicity.

MnSOD has a leader sequence to target mitochondria [mitochondrial targeting signal (MTS)]. This targeting signal translates to an oligopeptide consisting of 24 amino acids (14). The gene is transcribed in the nucleus, translated in the cytosol, and transported into mitochondria, where the precursor is cleaved and the protein undergoes maturation (22, 26). The localization of MnSOD in mitochondria is dependent on the presence of the signal. However, whether the enzyme could have an antioxidative function when it is present in the cytosol remains unclear.

In these studies, we examine the role of mitochondria-localized MnSOD in prevention against H/R-induced oxidative injuries, using a human pancreatic tumor-derived cell line, KP4, following H/R treatment. To elucidate further the significance of mitochondrial localization, MnSOD without the MTS gene was also tested using transfection in the same cell system.

MATERIALS AND METHODS

Cell lines

A pancreatic cancer cell line, KP4 (28), was purchased from the Riken Cell Bank (Tsukuba, Japan). pCR3.1-Uni plasmid (Invitrogen, Carlsbad, CA, U.S.A.) containing a sense human MnSOD cDNA insert was a kind gift of Dr. Akashi (National Institute of Radiological Sciences, Chiba, Japan) (27). A sequence analysis of the MnSOD gene in the construct showed that the sequence was identical to the accession number Y00472, except that C (nucleotide 113) was changed to T, and C (nucleotide 529) was changed to G, which changed alanine to valine and glutamine to glutamic acid, respectively (27). The KP4 cell was transfected using the GenePORTER transfection procedure (Gene Therapy Systems, San Diego, CA, U.S.A.) according to the manufacturer's instructions. In brief, cells were plated for 24 h before transfection at 60% confluence in a 60-mm dish. The cells were stably transfected with 5 μg of pCR3.1-Uni plasmids containing a sense human MnSOD cDNA insert, and linearized by Sca I, in a serum-free Dulbecco's modified Eagle medium (DMEM) (Life Technologies, Inc., Grand Island, NY, U.S.A.). The cells were also transfected with the same human MnSOD construct, but without an MTS [mito(−) MnSOD], which encodes 24 amino acids. The controls were transfected with pCR3.1-Uni plasmids without a human MnSOD cDNA insert and linearized by Sca I. Stable clones of both MnSOD and control plasmid transfectants were selected with Geneticin (Life Technologies, Inc.) at a final concentration of 500 μg/ml. Selected cellular clones that expressed MnSOD (MnSOD-5, -9, and -10), MnSOD without a targeting precursor [mito(−)-4, -6], selectable marker alone (vec-1 and -2),

and the parental cell (KP4) were used in all of the experiments. Selected clones were routinely maintained in DMEM containing 10% fetal bovine serum (JRH Biosciences, Lenexa, KS, U.S.A.) and 500 μg/ml Geneticin at 37°C in humidified air containing 5% CO_2.

To identify the localization of MnSOD and mito(−) MnSOD, KP4 cells were also transfected with pEGFP expression plasmid with the *MnSOD* gene or the *MnSOD* gene lacking MTS, which encodes the entire open reading frame of MnSOD or the MnSOD lacking a mitochondria targeting peptide, and also the mitochondria targeting peptide alone. To construct pEGFP expression plasmids, the cDNAs were incised with *Eco* RI and *Hind* III from the PCR products and inserted into the pEGFP-N1 expression vector (Clontech, San Diego, CA, U.S.A.). The construct was transformed into an XL1 Blue competent cell (Stratagene, La Jolla, CA, U.S.A.) and purified with a QIAFilter Plasmid Kit (QIAGEN, Valencia, CA, U.S.A.). The product was then transfected into cells using the GenePORTER 2 (Gene Therapy Systems), using the same method as described in the pCR3.1-Uni plasmid transfection procedure above. The transfected cells were visualized using a CSU-10 confocal laser scanning unit (Yokogawa Electric Co., Tokyo, Japan) coupled to an IX90 inverted microscope with a UPlanAPO X40 objective lens (Olympus Optical Co., Tokyo, Japan), and a C5810–01 color chilled 3CCD camera (Hamamatsu Photonics K. K., Hamamatsu, Japan). The cells were excited at 488 nm, and the emission was filtered using a 515-nm barrier filter. To ascertain localization of mitochondria, the cells were stained with MitoTracker Red CMXRos (Molecular Probes, Eugene, OR, U.S.A.), then visualized using a confocal laser scanning microscope excited at 488 nm, whereas the emission was filtered using a 580-nm barrier filter. A merged double image of (GFP) and MitoTracker was taken using a confocal laser scanning microscope excited at 488 nm, and the emission was filtered using a double-window barrier filter, of which the ranges were 510–590 and 580–620 nm.

In vitro *biological experimental system for hypoxia and PO_2 measurement system*

Biological experiments were performed in a hypoxic chamber [Anaerobic System MIP-1025 (Forma Scientific, Marietta, OH, U.S.A.)], which was specially modified to culture mammalian cells. The conditions inside the chamber were maintained with 95% humidified nitrogen plus 5% CO_2. The medium PO_2 in a representative flask was measured with MT 5000S (MTGiken, Tokyo, Japan), which was designed and made especially for our experimental system. This equipment included a small electrode (0.2 mm in diameter), which could detect PO_2 at a level as low as 0.1 mm Hg. A hypoxic condition of <8 mm Hg was maintained throughout the experiments. For H/R treatment, cells were maintained in hypoxia for 24 h followed by subsequent exposure to air.

Superoxide dismutase (SOD) activity gel assay

A nondenatured gel assay for SOD activity was performed according to a previously described method (3) with slight modifications. Cells were sonicated in a 50 m*M* potassium phosphate buffer (pH 7.8). Fifty micrograms of protein per lane was electrophoresed through a nondissociating riboflavin gel consisting of 5% stacking gel (pH 6.8) and 12% running gel (pH 8.8) at 4°C. To visualize SOD activity, gels were first incubated in 2.43 m*M* nitro blue tetrazolium (Wako Pure Chemical Industries, Ltd., Osaka, Japan) in deionized water for 20 min, and then in 0.028 m*M* riboflavin (Wako Pure Chemical Industries, Ltd.) and 280 m*M* TEMED (*N,N,N′,N′*-tetramethyl ethylenediamine; Sigma Chemical Co., St. Louis, MO, U.S.A.) in a 50 m*M* potassium phosphate buffer (pH 7.8) for 15 min in the dark. Gels were then washed in deionized water and illuminated under a fluorescent light until clear zones of SOD activity were evident. The images were obtained as TIFF files by a CCD camera in connection with a Power Macintosh G4 (Apple Computer, Inc., Cupertino, CA, U.S.A.). The bands of MnSOD were quantified by NIH Image 1.61, which is available on the Internet via a file-transfer protocol from http://rsb.info.nih.gov/nih-image/download.html. The MnSOD activity of the parental cell was used as the reference, and the relative MnSOD activities of other cells were normalized to those in the parental cells. The mean of the integrated density obtained from three independent experiments was used as a representative value for the experiment.

RT-PCR detection in MnSOD cells and mito(−) cells

Total RNA was isolated from cultured cells using the acid guanidinium–phenol–chloroform method (9). First-strand cDNA was synthesized using Moloney leukemia virus reverse transcriptase (TOYOBO, Tokyo, Japan) with an antisense primer, MnGPB 5′ CCCGAATTCCCTTTTTGCAAGCCATGTATCT 3′. A subsequent PCR was then performed using the same antisense primer, MnGPB, and a sense primer, MnGPA 5′ GGGAAGCTTTGGCTTCGGCAGCGGCTTCAG 3′, which is for detecting a whole range of normal MnSOD mRNA, or a sense primer, Mnmt-GPA 5′ GGGAAGCTTATGAAGCACAGCCTCCCCGACCTG 3′, which is for detecting MnSOD lacking MTS mRNA, using ExTaq DNA polymerase (TaKaRa, Tokyo, Japan) (Fig. 1). PCR was conducted in a PerkinElmer Cetus Thermal Cycler for 31 cycles. After 5 min at 94°C and 5 min at 60°C, amplification was performed for a cycling profile consisting of extension at 72°C for 1 min, denaturation at 94°C for 30 s, and annealing at 60°C for 30 s, followed by final extension at 72°C for 10 min. The PCR products were analyzed electrophoretically in a 1.5% agarose gel with ethidium bromide staining. An image was obtained, and the bands were quantified with an image quantifier (440CF; Kodak, New Haven, CT, U.S.A.)

Microscopic assessment of nuclear chromatin condensation and fragmentation

Cells grown on glass-bottom (35 mm) dishes (MatTek Corp., Ashland, MA, U.S.A.) were stained with a fluorescent dye, Hoechst 33342 (Molecular Probes). At 0, 0.25, 0.5, 1, 3, and 5 h after 1 day of hypoxia, the cells were fixed for 30 min in a solution containing 4% formaldehyde in phosphate-buffered saline (PBS), and then incubated in PBS with 1 μg/ml of the dye for 30 min. The cells were washed twice

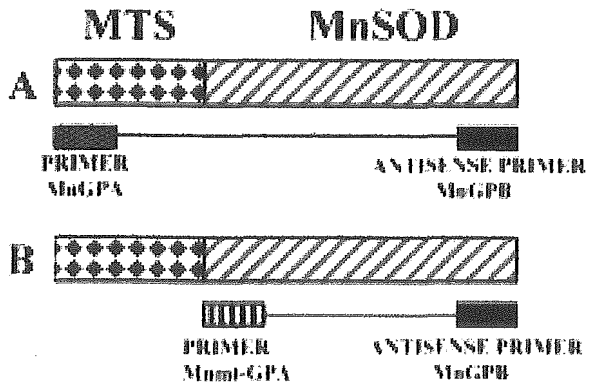

FIG. 1. Schematic diagram of MnSOD gene and primer setting. **(A)** Construct and primer range for MnSOD and primers used to generate and detect full-length MnSOD cDNA and mRNA. **(B)** Construct of the full-length MnSOD and primers used to generate and detect MTS-lacking MnSOD cDNA and mRNA.

with PBS and then twice with water. Fluorescence was visualized using an IX90 inverted microscope with a UPlanAPO 20× objective lens (Olympus Optical Co.). The dye was excited at 340 nm, and the emission was filtered with a 510-nm barrier filter. Photographs of microscope fields were taken using a C5810–01 color chilled 3CCD camera (Hamamatsu Photonics K.K.). More than 500 cells per culture dish were counted, and counts were made in three separate cultures per each H/R treatment. Analyses were performed without any knowledge of the H/R treatment history of the culture dishes. The percentage of apoptotic cells (apoptotic index) in each culture dish was determined.

Bioimaging of nitric oxide (NO)

Diaminofluoresceins (DAFs) (Daiichi Pure Chemicals, Tokyo, Japan) are fluorescent indicators for NO (17). They do not react with NO itself, but with NO+ equivalents, such as nitric trioxide (N_2O_3), which are produced by autoxidation of NO. Diaminofluorescein-FM diacetate (DAF-FM DA), which was a kind gift from Daiichi Pure Chemicals, is a newly synthesized DAF, which permeates well into cells and is quickly converted into water-soluble DAF-FM by esterases in the cytosol, where the dye can remain for a long time. Under aerobic conditions, DAF-FM traps NO to yield highly fluorescent triazofluoresceins (DAF-FM Ts) by nitrosation and dehydration. DAF-FM Ts are not formed in the presence of NO. Glass-bottom (35 mm) dishes (MatTek Corp.) with monolayers were prepared for staining with DAF-FM DA. At 0, 1, 2, 3, and 6 h after a H/R treatment, the cell culture medium was replaced with a modified Hanks' balanced salt solution containing 10.0 m*M* HEPES, 1.0 m*M* $MgCl_2$, 2 m*M* $CaCl_2$, and 2.7 m*M* glucose adjusted to pH 7.3 ± 0.05. The cells were then loaded with 10 μ*M* DAF-FM DA by incubation for 30 min at 37°C. Bioimages of DAF-FM DA were acquired using a CSU-10 confocal laser scanning unit (Yokogawa Electric Co.) coupled to an IX90 inverted microscope with UPlanAPO X20 objective lens (Olympus Optical Co.) and C5810–01 color chilled 3CCD camera (Hamamatsu Photonics. K.K.). The DAF-FM DA was excited at 488 nm, and the emission was filtered using a 515-nm barrier filter. The intensity of the laser beam, the exposure time of the 3CCD camera, and the gain of the amplifier were held at 500 μW, 1.0 s, and 18 db, respectively, to allow quantitative comparisons of the relative fluorescent intensity of the cells between groups. Cells were chosen and scanned at more than three spots for analysis on a random basis. The values for the average fluorescence intensity per cell were obtained using IPLab Spectrum version 3.0 (Scanalystics Inc., Fairfax, VA, U.S.A.) software with some modification of the program by the author (H.J.M). The fluorescent intensity (which was acquired by confocal laser microscopy and analyzed by computer) following H/R treatment divided by the intensity of no-treatment intact cells was calculated as the relative fluorescent intensity, which indicates the "increment" of the intensity induced by H/R treatment in each cell. Note that the relative fluorescent intensity is *not* the ratio of the fluorescent intensity to the control plasmid transfected cells or parental cells.

Relative levels of mitochondrial ROS

Dihydrorhodamine 123 (dhRho) (Molecular Probes) is an oxidation-sensitive lipophilic dye that enters a cell and fluoresces when oxidized by mitochondrial ROS to the positively charged rhodamine 123 derivatives. The relative level of mitochondrial ROS loaded with dhRho was quantified by a confocal laser microscope image using the same procedures described for DAF measurements, except that the final concentration of the dye used in the study was 10 μg/ml.

Immunofluorescent staining for 4-hydroxy-2-nonenal (HNE)

Glass-bottom (35 mm) dishes (MatTek Corp.) with monolayers were prepared for immunofluorescent staining with a monoclonal antibody directed against proteins modified by the major membrane lipid peroxidation product, HNE. This monoclonal antibody (NOF Corp., Tokyo, Japan), specific for HNE-modified proteins, was raised by immunizing mice with an HNE-modified keyhole limpet hemocyanin conjugate (40). The antibody was tested for cross-reactivity toward glutaraldehyde, formaldehyde, 1-hexanal, 2-hexanal, 4-hydroxy-2-hexanal, and 2-nonenal. Enzyme-linked immunosorbent assays with these potential competitors were performed. The results indicated that the anti-HNE antibody is highly specific to HNE-derived modifications to protein. At 0, 1, 2, 3, and 6 h after the H/R treatment, cells were fixed with 4% formaldehyde/PBS at room temperature for 30 min and then rinsed twice with PBS, and membranes were permeabilized by incubation in 95% ethanol with 5% acetic acid for 10 min. After washing with PBS twice, the cells were incubated for 4 min in a blocking solution(1% bovine serum albumin in PBS) and for 1 h in anti-HNE mouse monoclonal antibody at a dilution factor of 1:200. The cells were rinsed twice with 0.1% bovine serum albumin in PBS and reincubated with Alexa Fluor 488 goat anti-mouse IgG (H+L) conjugate (Molecular Probes) for 1 h at room temperature. Image acquisition and analysis were similar to that of DAF-FM DA, except that the exposure time of the 3CCD camera was 10 s.

Statistical analysis

A statistical analysis was performed by an analysis of variance, followed by Fisher's post hoc tests. A p value of <0.05 was considered to be statistically significant. Data were presented as the means ± SE. Calculations were performed with a statistical package, StatView 5.0J (SAS Institute Inc., Cary, NC, U.S.A.), on a Power Macintosh G3 (Apple Computer, Inc.).

RESULTS

Isolation of KP4 transfectants expressing MnSOD and mito(−) MnSOD

The production of active MnSOD in these transfectants was investigated in cell lysates. The parent KP4 cells, two vector clone transfectants (vec-1 and -2) (from six clones), two mito(−) MnSOD clones [mito(−)-4 and -6] (from six clones), and three MnSOD clones (MnSOD-5, -9 and -10) (from 12 clones) were examined for MnSOD activity. The intensity of MnSOD was semiquantified from the captured image. MnSOD activity of the parental cells was normalized to 1, and the relative MnSOD activities of the other cells were calculated (Table 1). The increase in MnSOD activity in the clones MnSOD-5, -9, and -10 was clearly detectable, *i.e.,* the MnSOD activity in the MnSOD-transfected cells was greater than that in the control cells. The relative activities of MTS-lacking MnSOD [mito(−)] transfectants were also greater compared with that in the control cells, although they were generally slightly less than those in the MnSOD clones.

RT-PCR detection of mRNA in MnSOD cells and mito(−) cells

To ascertain the expression of MnSOD and MnSOD lacking MTS, total cellular RNA was first reverse-transcribed into cDNA with an antisense primer, MnGPB, and then subsequently amplified by PCR. To examine the full-range MnSOD including MTS gene expressions, a sense primer (MnGPA) and an antisense primer (MnGPB) were used for PCR amplification, whereas to examine the MnSOD without MTS gene expression, a sense primer (Mnmt-GPA) and an antisense primer (MnGPB) were used for PCR amplification (Fig. 1). Increased MnSOD mRNA levels were confirmed in MnSOD-5, -9, and -10 using the MnGPA primer (Fig. 2A). However,

TABLE 1. RELATIVE INTENSITY OF MNSOD ACTIVITY

Cell line	*Relative intensity*
KP4	1
Vec-1	1.091 ± 0.040
Vec-2	1.207 ± 0.292
Mito(−)-4	2.320 ± 0.494
Mito(−)-6	1.861 ± 0.191
MnSOD-5	2.471 ± 0.362
MnSOD-9	3.024 ± 0.482
MnSOD-10	2.570 ± 0.505

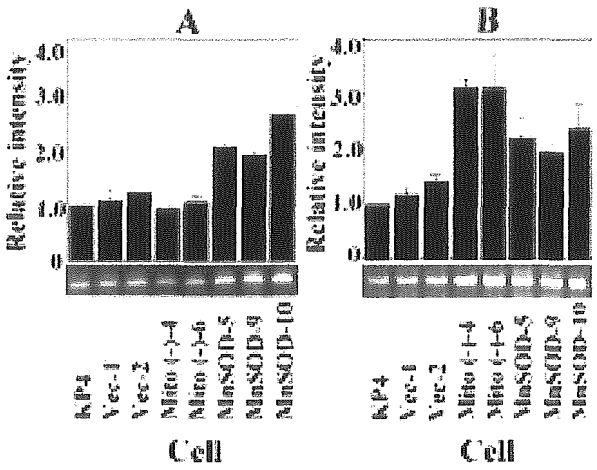

FIG. 2. RT-PCR detecting mRNA of the full length of normal MnSOD, or MTS-lacking MnSOD. (A) The full-length MnSOD including MTS gene expression, a sense primer (MnGPA), and an antisense primer (MnGPB) were used for PCR amplification. The full-length mRNA levels were higher in MnSOD-5, -9, -10 compared with that in the controls and mito(−) clones. **(B)** MnSOD without MTS, a sense primer (Mnmt-GPA), and an antisense primer (MnGPB) were used for the PCR amplification. The transfected mRNA was higher in MnSOD-5, -9, -10, mito(−) -4 and -6 transfectants, compared with the untransfected and vector alone controls.

when the Mnmt-GPA primer was used, not only did the mRNA for MnSOD-5, -9, and -10 increase, but higher mRNA levels of the MnSOD products for mito(−)-4 and -6 transfectants were observed (Fig. 2B). These results are consistent with those found for MnSOD activity and demonstrate that the transfection of MnSOD lacking MTS vectors was successful in mito(−) -4 and -6 transfectants.

Effect of MnSOD on H/R-induced apoptotic cell death

To determine the effect of H/R treatment on apoptotic cell death, we performed a microscopic assessment of nuclear chromatin condensation and fragmentation assay using Hoechst 33342 staining. For control experiments, we examined the change in the apoptotic index (number of apoptotic cells/500 cells counted) in air (Fig. 3A) or hypoxic conditions alone (Fig. 3B). As shown in Fig. 3, in cells grown up to 5 days in either air or hypoxic conditions, no increase in the apoptotic index was observed. In H/R experiments (Fig. 4), the apoptotic index was determined in cells cultured in air for 0, 0.25, 0.5, 1, 3, and 5 days after the 1-day hypoxia treatment. Except for MnSOD-5, -9, and -10, the apoptotic index significantly increased at 1 day, and by 5 days declined to the control levels in all cells. The absolute number of apoptotic cells and the relative index, which was calculated as the ratio of apoptotic cell count on day 1 to that on day 0, are listed in Table 2. The results show that the relative apoptotic index was suppressed in the full-length MnSOD transfected cells compared with that of the KP4, vec-1 and -2, and mito(−) transfectants. This result indicates that only when MnSOD is

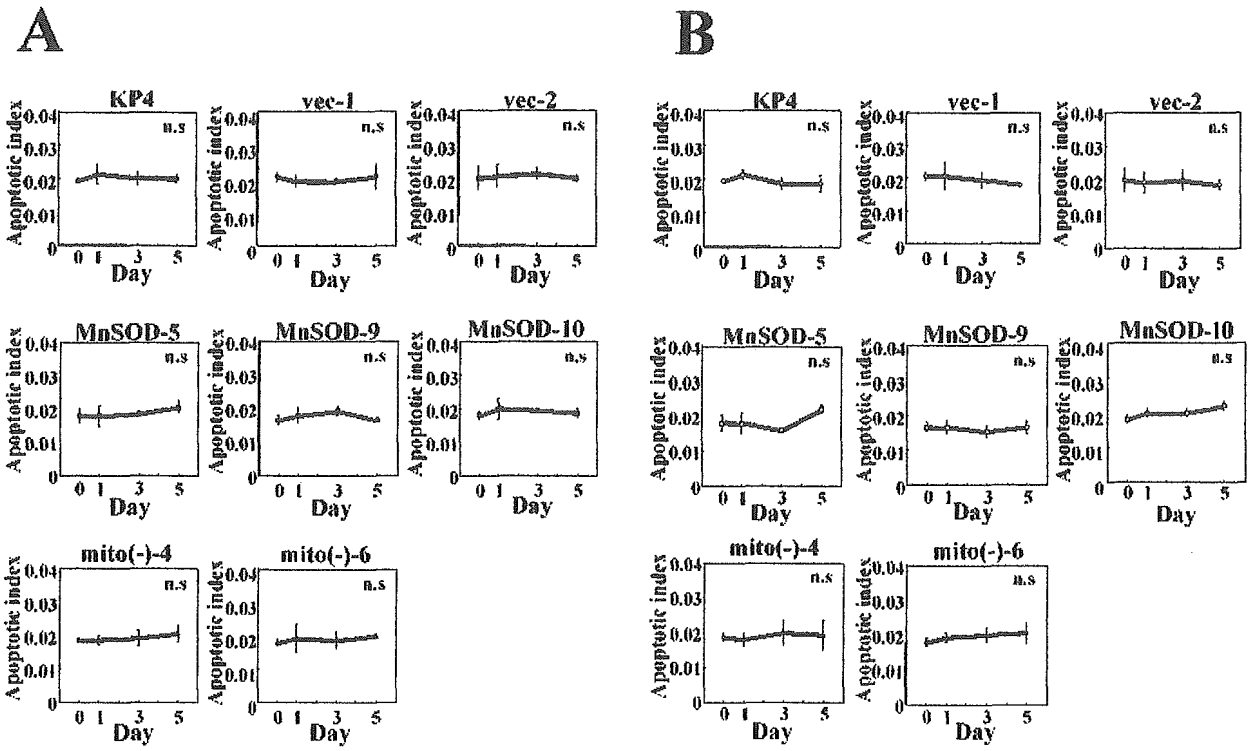

FIG. 3. No change in the apoptotic index as a function of time in air or hypoxic conditions. The change in apoptotic index (number of apoptotic cells/500 cells counted) in air **(A)** or hypoxia alone **(B)** is presented. n.s, not significant.

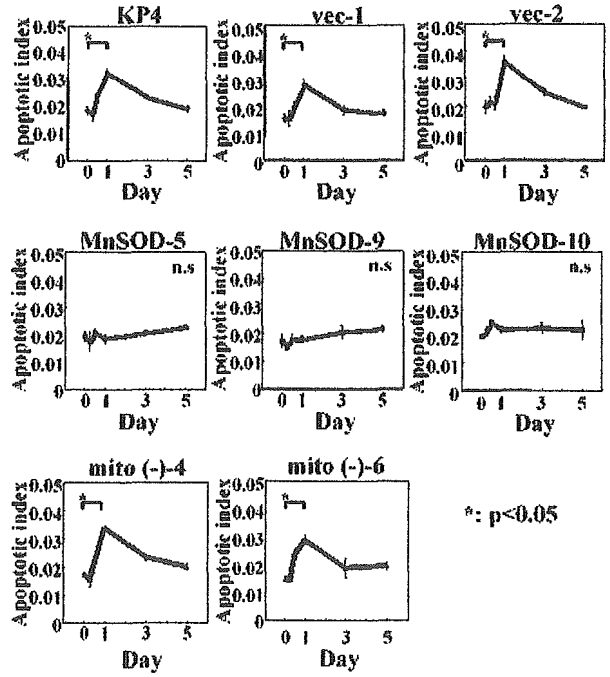

FIG. 4. Apoptotic index for H/R condition. The apoptotic index in each cell line at 0, 0.25, 0.5, 1, 3, and 5 days in air after 1 day of hypoxia treatment (H/R treatment) was determined. With the exception of MnSOD-5, -9, and -10, the apoptotic index increased to a maximum in 1 day, followed by a decline in all cells. The full-length MnSOD, and not MTS-lacking MnSOD, suppresses H/R treatment-induced apoptosis. n.s, not significant; $*p < 0.05$.

localized in the mitochondria can it suppress H/R-induced apoptosis.

MnSOD does not influence hypoxia-induced NO generation

To determine the effect of MnSOD on H/R treatment-induced intracellular NO generation, a dye sensitive to a change in the intracellular NO, DAF-FM DA, was used. To ascertain NO generation ability in every cell type, we irradiated cells with 15 Gy and examined NO generation at 2 h fol-

TABLE 2. NUMBER OF APOPTOTIC CELLS AND THE RELATIVE APOPTOTIC INDEX

Cell line	*Apoptotic cell day 1/day 0**	*Relative apoptotic index*
KP4	16.33 ± 0.88 / 9.33 ± 0.67	1.75 ± 0.09
Vec-1	14.00 ± 1.00 / 7.67 ± 0.67	1.83 ± 0.13
Vec-2	18.00 ± 1.00 / 9.67 ± 1.20	1.86 ± 0.10
Mito(−)-4	17.00 ± 0.00 / 8.67 ± 0.33	1.96 ± 0.00
Mito(−)-6	14.33 ± 0.88 / 7.33 ± 0.33	1.95 ± 0.12
MnSOD-5	9.33 ± 0.88 / 9.67 ± 0.88	0.97 ± 0.09†
MnSOD-9	9.00 ± 0.58 / 8.67 ± 1.20	1.04 ± 0.07†
MnSOD-10	11.00 ± 0.58 / 9.67 ± 0.33	1.14 ± 0.06†

*Absolute apoptotic cell number per 500 cells. Data shown in the table are the averages of three independent experiments.

†$p < 0.05$ versus KP4, $p < 0.05$ versus vec-1, $p < 0.05$ versus vec-2, $p < 0.05$ versus mito(−)-4, and $p < 0.05$ versus mito(−)-6.

lowing the irradiation. The results show 12–20% increases in NO generation in all cell types, indicating that every cell line has the ability to generate NO against oxidative stress (data not shown). In the next H/R experiments, the dye was loaded at 0, 1, 2, 3, and 6 h in air after 1 day of hypoxia treatment, and the images were acquired after 30 min of incubation. The fluorescent intensity was not changed after the H/R treatment in all cell types (Fig. 5). This result indicates that NO was not a major contributor of H/R-induced cell injury.

MnSOD suppresses H/R-induced mitochondrial ROS generation

To determine the effect of MnSOD on H/R-induced mitochondrial ROS generation, a dye sensitive to a change in mitochondrial ROS was used. For an analysis of the levels of mitochondrial ROS, we utilized the same analytic technique used for NO detection. The dye was loaded at 0, 1, 2, 3, and 6 h in air after 1 day of hypoxia treatment, and the images were acquired after 30 min of incubation. The change in the relative fluorescent intensity is shown in Fig. 6. This result shows that the relative fluorescent intensity of the dhRho was reduced in the MnSOD-transfected cells compared with the KP4, vec-1, and -2 cells, indicating that MnSOD suppresses H/R treatment-induced ROS generation in mitochondria. In addition, the change in ROS in the mito(−) cells following the H/R treatment was similar to that of the control and vector cells, indicating MnSOD lacking MTS had no effect on H/R-induced mitochondrial ROS levels.

H/R induces lipid peroxidation

To determine if changes of mitochondrial ROS generation are accompanied by an increase in lipid peroxidation products, the levels of HNE-modified proteins were evaluated by immunohistochemical staining. Preliminary experiments showed that there was no significant change in HNE-modified protein-staining intensity among all cell types using the intact cells (data not shown). The change in the relative HNE-modified protein-staining intensity in each cell line, which was obtained at 0, 1, 2, 3, and 6 h in air after 1 day of hypoxia treatment, is shown in Fig. 7. The result shows that the relative HNE-modified protein-staining intensity was suppressed in the MnSOD-transfected cells, but not in vector alone or MnSOD lacking MTS transfected cells. These results indicate that normal MnSOD, and not MnSOD lacking MTS, suppresses the levels of the H/R treatment-induced formation of intracellular HNE-modified proteins.

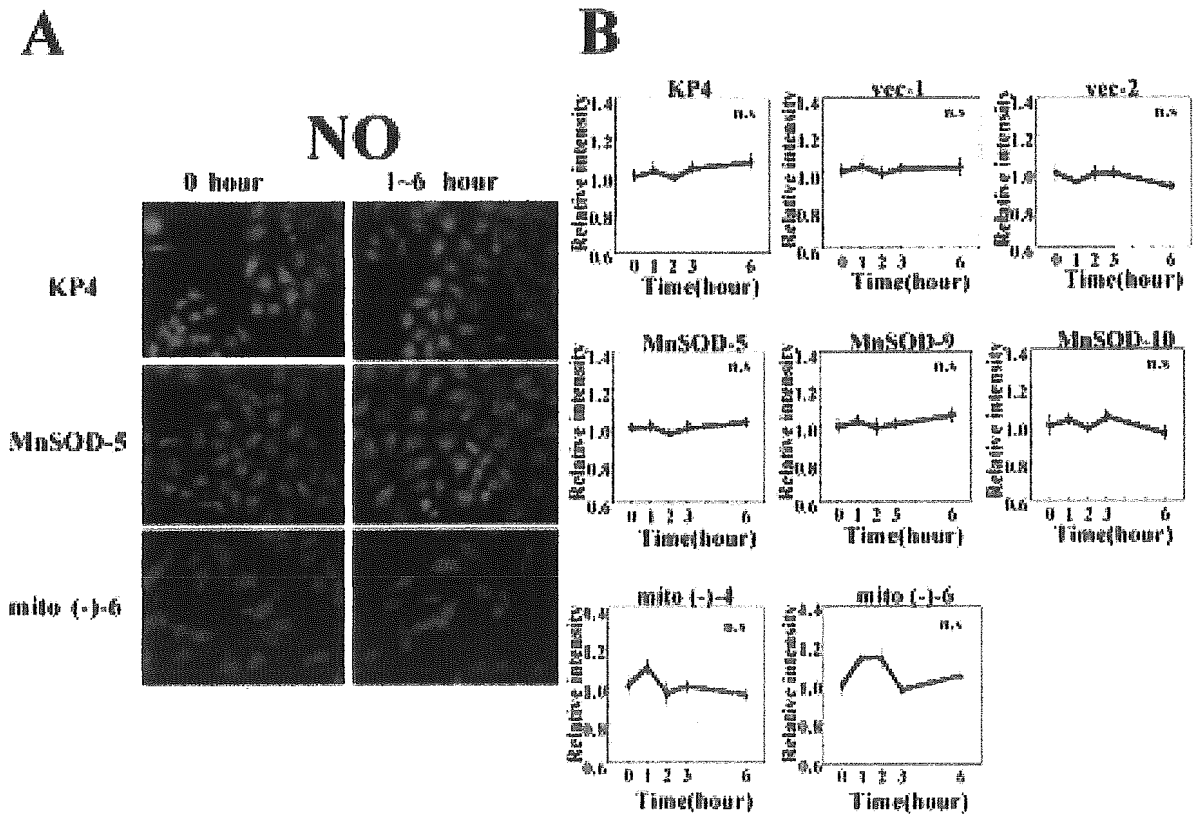

FIG. 5. Intracellular NO generation. The intracellular NO generation in each cell line at 0, 1, 2, 3, and 6 h in air after 1 day of hypoxia treatment (H/R treatment) was determined. No increase in the intracelluar NO levels was observed in all cell lines examined. The apparent increase in NO level did not achieve statical significance. **(A)** Representative photographs of cell stained with DAF. **(B)** Relative fluorescent intensity of DAF versus time (hours) in air following 1 day of hypoxia treatment (H/R treatment). n.s, not significant.

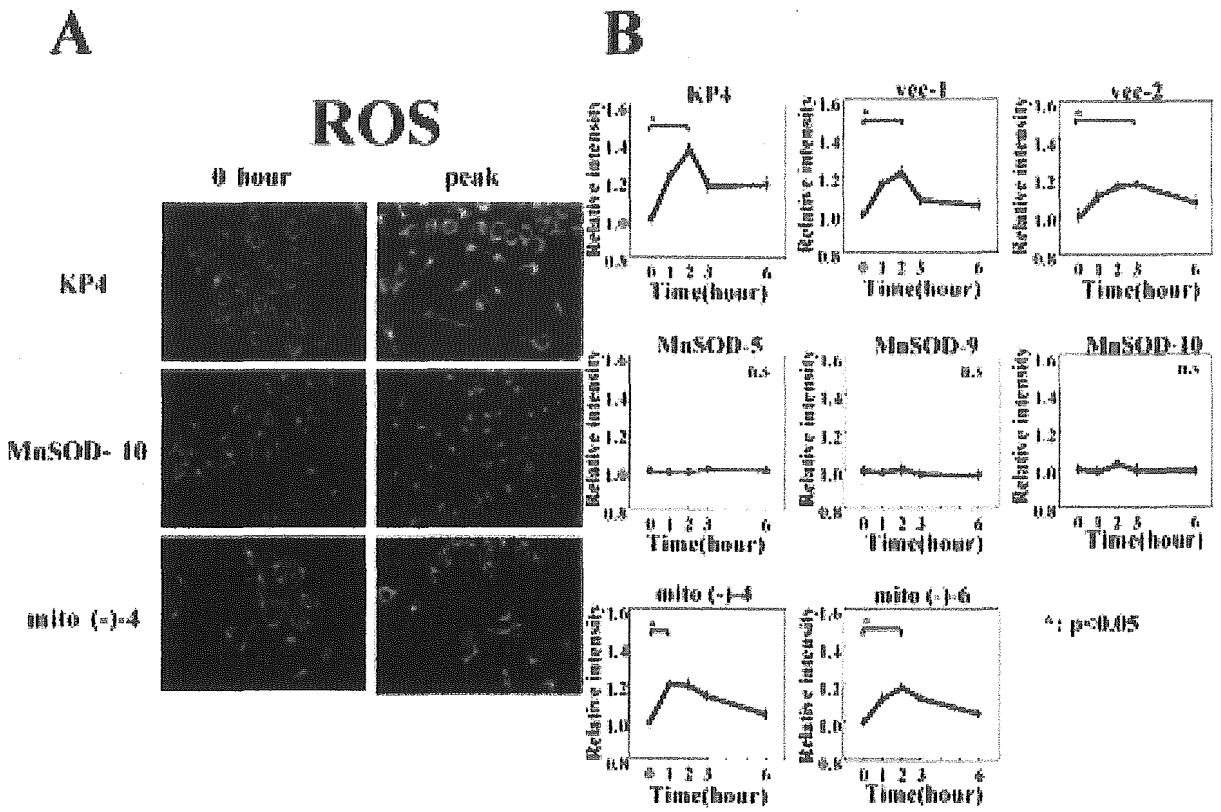

FIG. 6. Mitochondrial ROS generation. The levels of ROS in mitochondria in each cell line at 0, 1, 2, 3, and 6 h in air after 1 day of hypoxia treatment (H/R treatment) were determined. The relative fluorescent intensity of the dhRho was reduced in the MnSOD transfected cells compared with the KP4, vec-1 and -2, and mito(−) cells. **(A)** Representative images of cells examined for dhRho, at 0 h or at the peak times. **(B)** Relative fluorescent intensity of dhRho versus time (hours) in air following 1 day of hypoxia treatment (H/R treatment). n.s, not significant; $*p < 0.05$.

Correlation between mitochondrial ROS, intracellular lipid peroxidation products, and cell death

To understand better the relationship between mitochondrial ROS, intracellular lipid peroxidation, and cell death, we used a scattergram to plot (a) the relative apoptotic index against the relative dhRho (ROS) staining intensity, (b) the relative apoptotic index against the relative HNE-modified protein-staining intensity, and (c) the relative HNE-modified protein-staining intensity against the relative ROS staining intensity, and then analyzed the data using linear regression analysis. Figure 8A shows a linear-regression analysis of the relative apoptotic index against the relative mitochondrial ROS staining intensity (r = 0.818, p = 0.018). Figure 8B shows a linear-regression analysis of the relative apoptotic index versus the relative HNE-modified protein-staining intensity ($r = 0.933$, $p = 0.018$). These results show a strong positive correlation between the mitochondrial ROS, the intracellular lipid peroxidation products, and apoptosis. Figure 8C illustrates a linear-regression analysis of the relative ROS staining intensity versus the HNE-modified protein-staining intensity ($r = -0.856$, $p = 0.020$), indicating a correlation between the relative ROS staining intensity and that of HNE-modified protein adducts. Thus, intracellular mitochondrial ROS staining intensity and relative HNE-modified protein-staining intensity have a strong correlation with apoptosis, and there is a strong correlation with mitochondrial ROS staining intensity and HNE-modified protein-staining intensity.

Localization of MnSOD, MnSOD lacking MTS, and MTS signal only in KP4 cells

To examine localization of MnSOD, MnSOD lacking MTS [MnSOD mito(−)], and MTS signal alone (Mito signal), the cDNA was linked with the pEGFP vector and then transfected with KP4 cells. To localize mitochondria, the same cells were stained with MitoTracker Red CMXRos. A merged double image of GFP and MitoTracker was made to verify coexistence of MnSOD, MnSOD lacking MTS, or MTS alone in mitochondria. Figure 9 shows that MnSOD was localized in mitochondria, as shown by the color yellow (green plus red) in the double image of pEGFP and Mitotracker. A similar image was taken for MTS alone (Mito signal) in the double image, where a yellow color is clearly shown. However, for MTS-lacking MnSOD [MnSOD mito(−)], only a few yellow color regions can be seen in the double color picture, indicating the most of the MnSOD lacking MTS was localized in cytosol, although the fluorescent intensity of pEGFP in the image is unclear or obscure in the cytosol.

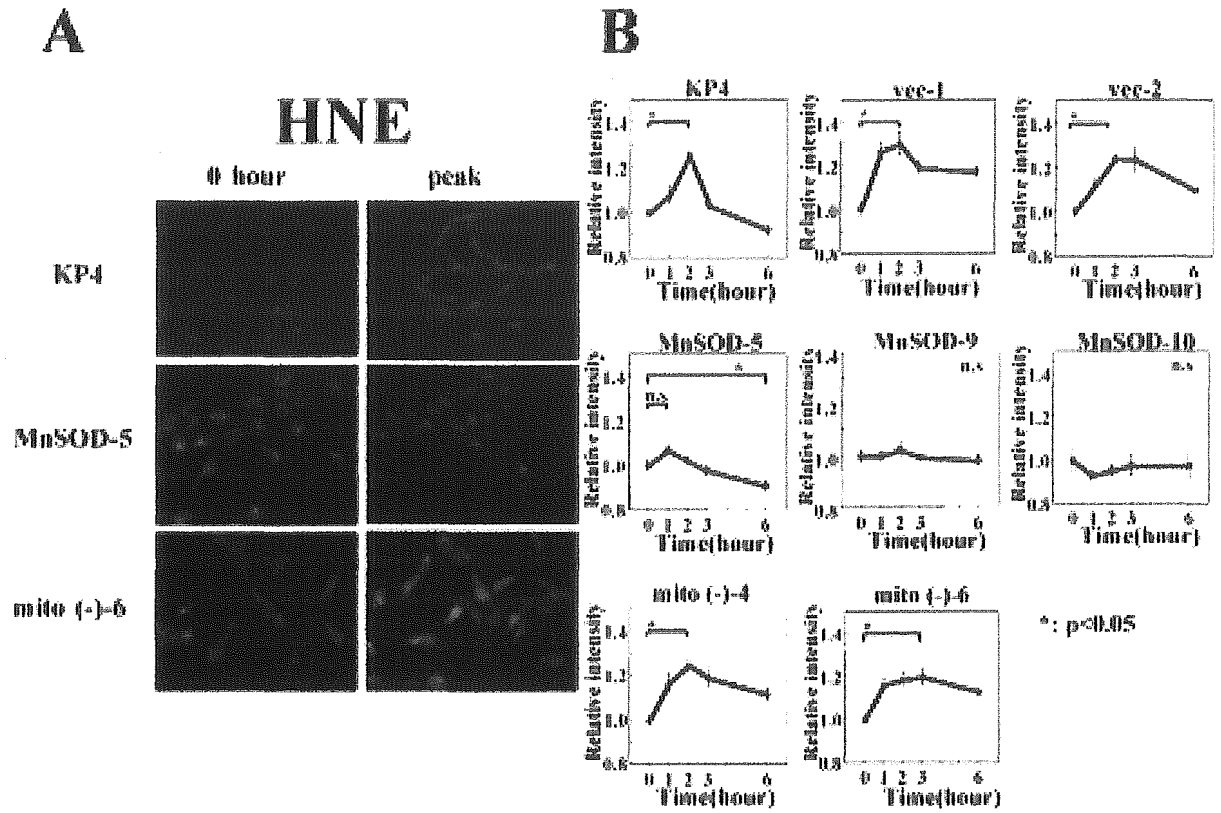

FIG. 7. Intracellular HNE adducts. The intracellular levels of HNE protein adducts in each cell line at 0, 1, 2, 3, and 6 h in air after 1 day of hypoxia treatment (H/R treatment) were determined. **(A)** Representative photographs of cell staining with an antibody against HNE protein adducts at 0 h or peak hours. **(B)** Relative fluorescent intensity of HNE protein adducts versus time (hours) in air following 1 day of hypoxia treatment (H/R treatment). n.s, not significant; $*p < 0.05$.

DISCUSSION

Using a human pancreatic tumor cell line, KP4, we first examined the effects of H/R on ROS production, lipid peroxidation, and cellular viability following 1 day of hypoxia and subsequent exposure to air. The results show that H/R increased ROS, lipid peroxidation, and apoptosis, although the apoptosis frequency was small. In this study, we investigated whether an enhanced expression of mitochondrial MnSOD, a superoxide-scavenging enzyme, can protect cells against H/R.

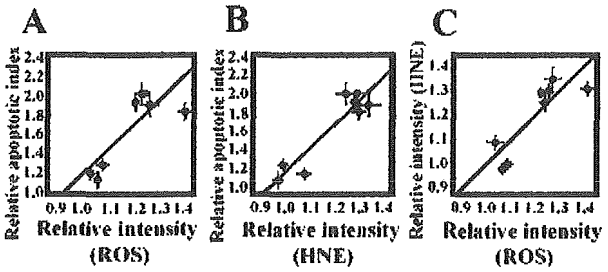

FIG. 8. Correlation between mitochondrial ROS, intracellular lipid peroxidation protein adducts, and cell death. (A) Linear-regression analysis showing the relationship between the relative apoptosis index and the relative dhRho staining intensity (mitochondrial ROS) after H/R treatment ($r = 0.818, p = 0.018$). **(B)** Relationship between the relative apoptosis index and the relative HNE protein-adducts staining intensity (intracellular lipid peroxidation products) ($r = 0.933, p = 0.018$). **(C)** Relationship between the relative dhRho staining intensity and the relative HNE protein adducts staining ($r = -0.856, p = 0.020$). Mitochondrial ROS, intracellular lipid peroxidation products, and apoptosis have a strong correlation with each other.

We found that H/R-produced apoptosis is suppressed by MnSOD, but not by mito(−) MnSOD, which is not located in the mitochondria. These results signify the importance of mitochondrial localization of MnSOD. It has been shown that adenoviral gene transfer with MnSOD is effective in reducing the extent of *in vivo* I/R injury in the rat heart (1) and in mouse liver (50), but expression of copper/zinc SOD (Cu/ZnSOD) did not function in protection in the mouse liver model (50). Given the fact that the MnSOD and Cu/ZnSOD used in these studies were mainly expressed in the mitochondria and cytosol, respectively, these results are consistent with our results. Our results further indicate that not only is active MnSOD important, but also it must be located in the mitochondria for the observed protection.

The reaction between superoxide radicals and NO to form peroxynitrite is a subject under considerable study. Superoxide radicals can react at diffusion rates with NO to form peroxynitrite, a potent biological oxidant. In this study, however, we could not find evidence of further NO induction by hypoxia treatment. This is not surprising, because oxygen is an essential substrate for NO synthesis. Our results are also consistent with various other reports that indicate that hypoxia

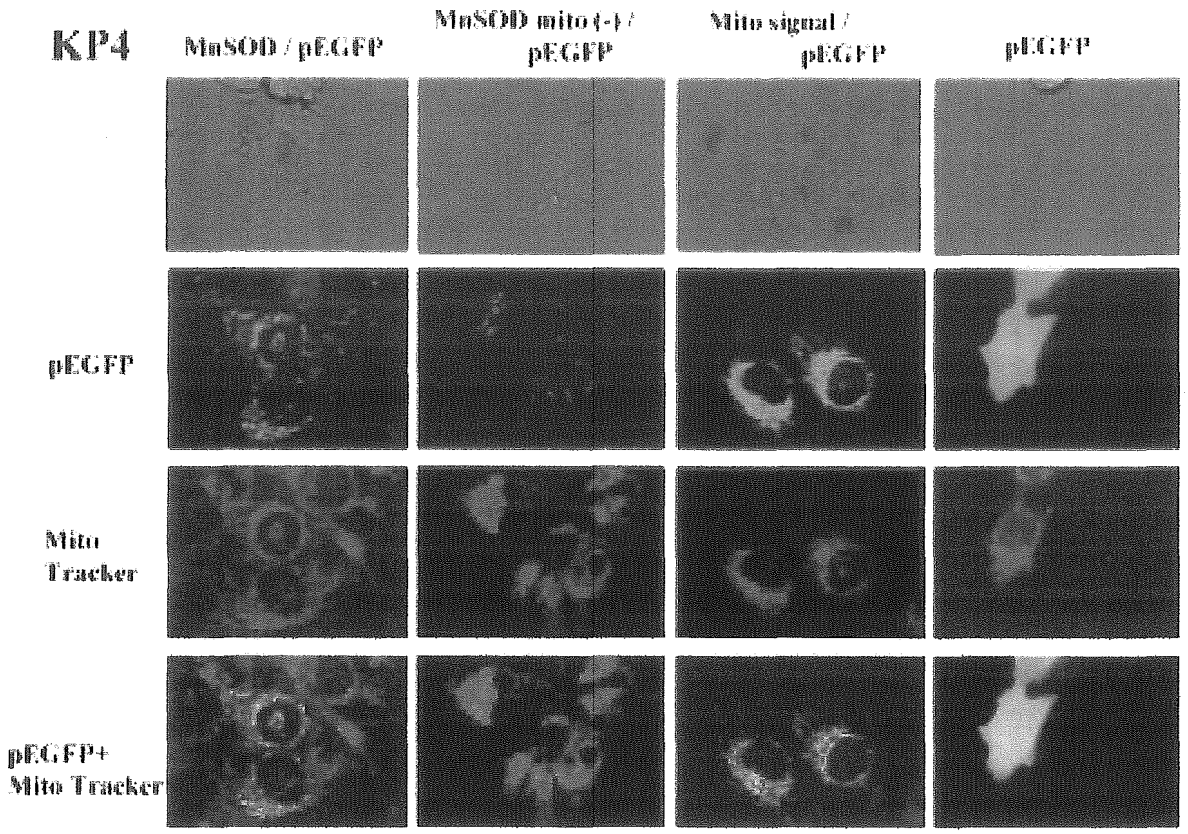

FIG. 9. Localization of MnSOD, MnSOD lacking MTS, and MTS alone in KP4 cells. Localization of full-length MnSOD, MnSOD lacking MTS [MnSOD mito (−)], and MTS signal alone (Mito signal) is shown. GFP was visualized using the pEGFP transfection sytem. To locate mitochondria, the same cells were stained with MitoTracker Red CMXRos. Merged double images of GFP and MitoTracker were made to identify MnSOD in mitochondria. MnSOD was localized in mitochondria, as shown by the yellow color (green plus red) in the double image of pEGFP and MitoTracker. A similar image was taken for MTS alone (Mito signal) in the double image, where a yellow color is clearly shown. However, for MTS lacking MnSOD [MnSOD mito (−)], only a few yellow color regions can be seen in the double color picture, indicating that most of the MnSOD lacking MTS was localized in cytosol, although the fluorescent intensity of pEGFP is unclear or obscure in cytosol in the picture.

limits NO synthesis even when NO synthase is overexpressed (for review, see 19). As ROS are increased without a concurrent increase in NO production in the H/R model, it is likely that the observed increase in HNE-modified proteins is mediated via hydroxyl radical generation. The finding that increased expression of MnSOD abolished the increased levels of HNE-modified proteins under H/R further supports this possibility.

Our results indicating that only MnSOD and not mito(−) transfectants suppress the formation of HNE-modified proteins suggest that superoxide production in the mitochondria is important for the production of HNE-modified proteins under conditions of H/R. Our results further indicate that the localization of active MnSOD in the mitochondrion is important for the suppression of ROS production and subsequent formation of HNE protein adducts. These results suggest that H/R-induced apoptosis is linked to the production of ROS and its toxic products.

Mitochondrial damage and the role of mitochondria in apoptosis are well established in various pathological conditions. However, it is largely unknown whether mitochondria are the sources or targets in such apoptosis events. Our results suggest that induction of oxidative injury in mitochondria is an upstream event leading to apoptosis in H/R-induced cell death.

Endogenous MnSOD is a nuclear-encoded protein that is cotranslationally transported into mitochondria where the signal peptide is removed and Mn is inserted to produce active proteins. The role of MnSOD in protecting against oxidative stress-mediated cell death has been demonstrated in organisms ranging from bacteria to mammals. In all studies reported thus far, it has been assumed that the effect of MnSOD is due to its location in mitochondria. However, the question remains to be investigated as to whether enzyme localized outside mitochondria has any protective effect. Our results reported here clearly demonstrate that expression of active MnSOD outside mitochondria was not effective. Although it is unclear how MnSOD located outside mitochondria acquires its Mn and proper conformation for its activity, our results from activity assay, mRNA RT-PCR assay, apoptosis observation, and colocalization studies (Table 1, Figs. 2, 4, and 9) provide strong support that active MnSOD outside mitochondria is not effective in protecting against H/R-induced apoptosis. Our GFP vector images (Fig. 9) show that

only small amounts of transfectants of MnSOD mito(−) are found in mitochondria. The distribution of GFP outside mitochondria of the MnSOD and Mito signal alone may indicate that the intensity of MnSOD lacking MTS was low because of a wide dispersion over cytosol. Although our finding that the MnSOD construct lacking MTS expresses active MnSOD protein outside mitochondria is unexpected; this phenomenon has been observed for other antioxidant enzymes as well. For example, Tamura *et al.*(37) demonstrated a much greater enhancement of cellular resistance to oxidant challenge by CHO cells by stable transfection with leader sequence of glutathione reductase (GR) cDNA than they observed in a construct lacking the MTS, which produced comparable increases in the total cellular GR activities, but did not increase mitochondrial GR activities (29, 37, 38). Arai *et al.* (2) demonstrated the effect of phospholipid hydroperoxide glutathione peroxidase, which is naturally synthesized as a long form (the L-form; 23 kDa) and a short form (the S-form; 20 kDa). The long form contains a mitochondrial targeting leader sequence, whereas the short form lacks the leader sequence. Cells transfected with the L-form containing vector were more resistant against oxidative stress, including potassium cyanide, rotenone (chemical hypoxia), and exogenous *tert*-butyl hydroperoxide oxidant injuries, compared with those cells transfected with the S-form containing vector (2). Wong (46) demonstrated that MnSOD without the mitochondrial leading targeting signal failed to protect against radiation, whereas the reduction of normal cytosolic Cu/ZnSOD or normally extracellularly expressed SOD to mitochondria with MTS resulted in protection against radiation. These results suggest that MnSOD, which is located in cytosol, does not function to prevent against H/R treatment-induced oxidative damage and cell death, and only when the enzyme is located in mitochondria does MnSOD have a function. Taken together, these data support the critical role of mitochondria localization of antioxidant enzymes for the protection against cellular injury from outside stress initiated in the mitochondrion.

In summary, the findings shown in study indicated that (a) H/R induced increased mitochondrial ROS production, lipid peroxidation protein-adducts, and subsequent apoptosis; (b) these processes were suppressed by active MnSOD in the mitochondria but not in the cytosol even when the MnSOD is active; and (c) the results support the overall hypothesis depicted in Fig. 10 showing that H/R triggers mitochondrial ROS production and generation of lipid peroxidation products, and subsequently accelerates cell death and its inhibition by MnSOD.

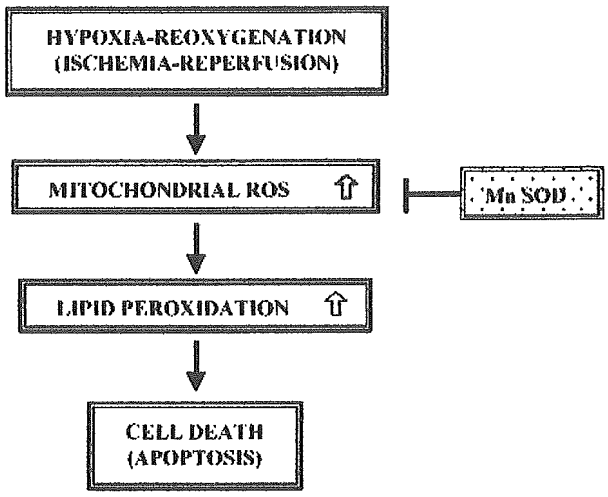

FIG. 10. Schematic diagram of a hypothesis on how ROS generation and lipid peroxidation products affect cell death (apoptosis) and its prevention by MnSOD after H/R treatment.

ACKNOWLEDGMENTS

The authors wish to thank Dr. Makoto Akashi (NIRS) for MnSOD cDNA, and Ms Chizuru Yamaguchi and Dr. Yoichiro Iwashita for technical assistance. This study was partially supported by "Ground Research Announcement for Space Utilization" promoted by Japan Space Forum, and The Nuclear Cross-Over Research Study, Grant-in Aid for Scientific Research (C) (2) #10671786, #12671844, #14207078, and #15659451 of Ministry of Education, Culture, Sports, Science and Technology, Japan.

ABBREVIATIONS

Cu/ZnSOD, copper/zinc superoxide dismutase; DAF, diaminofluorescein; DAF-FM DA, diaminofluorescein-FM diacetate; dhRho, dihydrorhodamine 123; DMEM, Dulbecco's modified Eagle medium; GFP, green fluorescent protein; GR, glutathione reductase; HNE, 4-hydroxy-2-nonenal; H/R, hypoxia followed by reoxygenation; I/R, ischemia/reperfusion; mito(−), lacking MTS; mito(−)-, MTS lacking MnSOD transfected cell clone; MnSOD, manganese superoxide dismutase (EC 1.15.1.1); MnSOD-, MnSOD transfected cell clone; MTS, mitochondrial targeting signal; NO, nitric oxide; PBS, phosphate-buffered saline; ROS, reactive oxygen species; SOD, superoxide dismutase; vec-, vector alone transfected cell clone.

REFERENCES

1. Abunasra HJ, Smolenski RT, Morrison K, Yap J, Sheppard MN, O'Brien T, Suzuki K, Jayakumar J, and Yacoub MH. Efficacy of adenoviral gene transfer with manganese superoxide dismutase and endothelial nitric oxide synthase in reducing ischemia and reperfusion injury. *Eur J Cardiothorac Surg* 20: 153–158, 2001.
2. Arai M, Imai H, Koumura T, Yoshida M, Emoto K, Umeda M, Chiba N and Nakagawa Y. Mitochondrial phospholipid hydroperoxide glutathione peroxidase plays a major role in preventing oxidative injury to cells. *J Biol Chem* 274: 4924–4933, 1999.
3. Beauchamp C and Fridovich I. Superoxide dismutase: improved assays and an assay applicable to acrylamide gels. *Anal Biochem* 44: 276–287, 1971.
4. Bienvenu P, Caron L, Gasparutto D, and Kergonou JF. Assessing and counteracting the prooxidant effects of anticancer drugs. *EXS* 62: 257–265, 1992.

5. Boveris A and Cadenas E. Mitochondrial production of superoxide anions and its relationship to the antimycin insensitive respiration. *FEBS Lett* 1: 311–314, 1975.
6. Brown JM. Evidence for acutely hypoxic cells in mouse tumours, and a possible mechanism of reoxygenation. *Br J Radiol* 52: 650–656, 1979.
7. Brown JM. The hypoxic cell: a target for selective cancer therapy—eighteenth Bruce F. Cain Memorial Award lecture. *Cancer Res* 59: 5863–5870, 1999.
8. Carlioz A and Touati D. Isolation of superoxide dismutase mutants in *Escherichia coli:* is superoxide dismutase necessary for aerobic life? *EMBO J* 5: 623–630, 1986.
9. Chomczynski P and Sacchi N. Single-step method of RNA isolation by acid guanidinium thiocyanate–phenol–chloroform extraction. *Anal Biochem* 162: 156–159, 1987.
10. Engelhardt JF. Redox-mediated gene therapies for environmental injury: approaches and concepts. *Antioxid Redox Signal* 1: 5–27, 1999.
11. Farr SB, D'Ari R, and Touati D. Oxygen-dependent mutagenesis in *Escherichia coli* lacking superoxide dismutase. *Proc Natl Acad Sci USA* 83: 8268–8272, 1986.
12. Halliwell B and Gutteridge JMC. Free radicals, other reactive species and disease. In: *Free Radicals in Biology and Medicine,* 3rd edit., edited by Halliwell B and Gutteridge JMC. Oxford, U.K.: Oxford University Press, 1999, pp.617–783.
13. Hirose K, Longo DL, Oppenheim JJ, and Matsushima K. Overexpression of mitochondrial manganese superoxide dismutase promotes the survival of tumor cells exposed to interleukin-1, tumor necrosis factor, selected anticancer drugs, and ionizing radiation. *FASEB J* 7: 361–368, 1993.
14. Ho YS and Crapo JD Isolation and characterization of complementary DNAs encoding human manganese-containing superoxide dismutase. *FEBS Lett* 229: 256–260, 1988.
15. Kiningham KK, Oberley TD, Lin S, Mattingly CA, and St Clair DK. Overexpression of manganese superoxide dismutase protects against mitochondrial-initiated poly(ADP-ribose) polymerase-mediated cell death. *FASEB J* 13: 1601–1610, 1999.
16. Knisely JP and Rockwell S. Importance of hypoxia in the biology and treatment of brain tumors. *Neuroimaging Clin NAm* 12: 526–536, 2002.
17. Kojima H, Nakatsubo N, Kikuchi K, Kawahara S, Kirino Y, Nagoshi H, Hirata Y, and Nagano T. Detection and imaging of nitric oxide with novel fluorescent indicators: diaminofluoresceins. *Anal Chem* 70: 2446–2453, 1998.
18. Lebovitz RM, Zhang H, Vogel H, Cartwright J Jr, Dionne L, Lu N, Huang S, and Matzuk MM. Neurodegeneration, myocardial injury, and perinatal death in mitochondrial superoxide dismutase deficient mice. *Proc Natl Acad Sci U S A* 93: 9782–9787, 1996.
19. Le Cras TD and McMurtry IF. Nitric oxide production in the hypoxic lung. *Am J Physiol Lung Cell Mol Physiol* 280: L575–L582, 2001.
20. Lee JM, Zipfel GJ, and Choi DW. The changing landscape of ischaemic brain injury mechanisms. *Nature* 399 (6738 Suppl): A7–A14, 1999.
21. Li Y, Huang T-T, Carlson EJ, Melov S, Ursell PC, Olson JL, Noble LJ, Yoshimura MP, Berger C, Chan PH, Wallace DC, and Epstein CJ. Dilated cardiomyopathy and neonatal lethality in mutant mice lacking manganese superoxide dismutase. *Nat Genet* 11: 376–381, 1995.
22. Lithgow T. Targeting of proteins to mitochondria. *FEBS Lett* 476: 22–26, 2000.
23. Majima HJ, Oberley TD, Furukawa K, Mattson MP, Yen HC, Szweda LI, and St. Clair DK. Prevention of mitochondrial injury by manganese superoxide dismutase reveals a primary mechanism for alkaline-induced cell death. *J Biol Chem* 273: 8217–8224, 1998.
24. Mattson MP. Apoptosis in neurodegenerative disorders. *Nat Rev Mol Cell Biol* 1: 120–129, 2000.
25. Mattson MP, Duan W, Pedersen WA, and Culmsee C. Neurodegenerative disorders and ischemic brain diseases. *Apoptosis* 6: 69–81, 2001.
26. Mihara T and Onuma T. Cytoplasmic chaperons in precursor targeting to mitochondria: the role of MSF and hsp70. *Trends Cell Biol* 6: 104–108, 1996.
27. Motoori S, Majima HJ, Ebara M, Kato H, Hirai F, Kakinuma S, Yamaguchi C, Ozawa T, Nagano T, Tsujii H, and Saisho H. Overexpression of mitochondrial manganese superoxide dismutase protects against radiation-induced cell death in the human hepatocellular carcinoma cell line HLE. *Cancer Res* 61: 5382–5388, 2001.
28. Nishi Y, Haji M, Takayanagi R, Iguchi H, Shimazoe T, Hirata J, and Nawata H. Establishment of characterization of PTHrP-producing human pancreatic cancer cell line. *Int J Oncol* 5: 33–39, 1994.
29. O'Donovan DJ, Katkin JP, Tamura T, Husser R, Xu X, Smith CV, and Welty SE. Gene transfer of mitochondrially targeted glutathione reductase protects H441 cells from *t*-butyl hydroperoxide-induced oxidant stresses. *Am J Respir Cell Mol Biol* 20: 256–263, 1999.
30. Riley PA. Free radicals in biology: oxidative stress and the effects of ionizing radiation. *Int J Radiat Biol* 65: 27–33, 1994.
31. Rofstad EK. Microenvironment-induced cancer metastasis. *Int J Radiat Biol* 76: 589–605, 2000.
32. St Clair DK, Oberley TD, and Ho Y-S. Overproduction of human Mn-superoxide dismutase modulates paraquat-mediated toxicity in mammalian cells. *FEBS Lett* 293: 199–203, 1991.
33. St. Clair DK, Wan XS, Oberley TD, Muse KE, and St Clair WH. Suppression of radiation-induced neoplastic transformation by overexpression of mitochondrial superoxide dismutase. *Mol Carcinog* 6: 238–242, 1992.
34. St Clair DK, Jordan JA, Wan S, and Gairola CG. Protective role of manganese superoxide dismutase against cigarette smoke-induced cytotoxicity. *J Toxicol Environ Health* 43: 239–249, 1994.
35. Sun J, Chen Y, Li M, and Ge Z. Role of antioxidant enzymes on ionizing radiation resistance. *Free Radic Biol Med* 24: 586–593, 1998.
36. Takeshige K and Minakami S. NADH- and NADPH-dependent formation of superoxide anions by bovine heart submitochondrial particles and NADH-ubiquinone reductase preparation. *Biochem J* 180: 129–135, 1979.
37. Tamura T, McMicken HW, Smith CV, and Hansen TN. Mitochondrial targeting of glutathione reductase requires a leader sequence. *Biochem Biophys Res Commun* 222: 659–663, 1996.

38. Tamura T, McMicken HW, Smith CV, and Hansen TN. Gene structure for mouse glutathione reductase, including a putative mitochondrial targeting signal. *Biochem Biophys Res Commun* 237: 419–422, 1997.
39. Thomlinson RH and Gray LH. The histological structure of some human lung cancers and the possible implications for radiotherapy. *Br J Cancer* 9: 539–549, 1955.
40. Toyokuni S, Miyake N, Hiai H, Hagiwara M, Kawakishi S, Osawa T, and Uchida K. The monoclonal antibody specific for the 4-hydroxy-2-nonenal histidine adduct. *FEBS Lett* 359: 189–191, 1995.
41. van Loon APGM, Pesold-Hurt B, and Schatz G. A yeast mutant lacking mitochondrial manganese-superoxide dismutase is hypersensitive to oxygen. *Proc Natl Acad Sci U S A* 83: 3820–3824, 1986.
42. van Putten LM. Tumor reoxygenation during fractionated radiotherapy: studies with a transplantable osteosarcoma. *Eur J Cancer* 4: 173–182, 1968.
43. Wallace DC. Mitochondrial DNA in aging and disease. *Sci Am* 277: 40–47, 1997.
44. Weisiger RA and Fridovich I. Mitochondrial superoxide disimutase. Site of synthesis and intramitochondrial localization. *J Biol Chem* 248: 4793–4796, 1973.
45. Wispe JR, Warner BB, Clark JC, Dey CR, Neuman J, Glasser SW, Crapo JD, Chang L-Y, and Whitsett JA. Human Mn-superoxide dismutase in pulmonary epithelial cells of transgenic mice confers protection from oxygen injury. *J Biol Chem* 267: 23937–23941, 1992.
46. Wong GH. Protective roles of cytokines against radiation: induction of mitochondrial MnSOD. *Biochim Biophys Acta* 1271: 205–209, 1995.
47. Wong GHW, Elwell JH, Oberley LW, and Goeddel DV. Manganous superoxide dismutase is essential for cellular resistance to cytotoxicity of tumor necrosis factor. *Cell* 58: 923–931, 1989.
48. Yen H-C, Oberley TD, Vichitbandha S, Ho Y-S, and St Clair DK. The protective role of manganese superoxide dismutase against adriamycin-induced acute cardiac toxicity in transgenic mice. *J Clin Invest* 98: 1253–1260, 1996.
49. Yen H-C, Nien C-Y, Majima HJ, Lee C-P, Chen S-Y, Wei J-S, and See L-C. Increase of lipid peroxidation by cisplatin in WI38 cells but in SV40-transformed WI38 cells. *J Biochem Mol Toxicol* 17: 39–46, 2003.
50. Zhou W, Zhang Y, Hosch MS, Lang A, Zwacka RM, and Engelhardt JF. Subcellular site of superoxide dismutase expression differentially controls AP-1 activity and injury in mouse liver following ischemia/reperfusion. *Hepatology* 33: 902–914, 2001.

Address reprint requests to:
Hideyuki J. Majima, D.D.S., Ph.D.
Department of Oncology and Department of Space Environmental Medicine
Kagoshima University Graduate School of Medical and Dental Sciences
Kagoshima 890-8544, Japan

E-mail: hmajima@denta.hal.kagoshima-u.ac.jp

Received for publication October 18, 2003; accepted February 19, 2004.

Evaluation of anti-platelet aggregatory effects of aspirin, cilostazol and ramatroban on platelet-rich plasma and whole blood

Hiroko Kariyazono[a], Kazuo Nakamura[a], Junko Arima[a], Osamu Ayukawa[a], Shunji Onimaru[a], Hiroshi Masuda[b], Yoshifumi Iguro[b], Hideyuki J. Majima[c], Ryuzo Sakata[b] and Katsushi Yamada[a]

To compare property in anti-platelet effects of aspirin (a cyclooxygenase inhibitor), cilostazol (a phosphodiesterase III inhibitor) and ramatroban (a specific thromboxane A_2 receptor antagonist), we measured human platelet-rich plasma (PRP) aggregation induced by adenosine diphosphate (ADP), collagen and arachidonic acid, and whole blood (WB) aggregation induced by ADP. The release of P-selectin, transforming growth factor-beta 1, and the formation of thromboxane A_2 in response to agonists were also investigated. Inhibitory effects of 100 μmol/l aspirin, 10 μmol/l cilostazol and 1 μmol/l ramatroban on 5 μmol/l ADP-induced PRP aggregation were similar. However, aspirin strongly inhibited thromboxane A_2 formation in response to 5 μmol/l ADP compared with other drugs. Inhibitory effects of 10 μmol/l cilostazol on PRP aggregation and the release of molecules were quite similar in responsiveness induced by the three agonists. Aspirin and cilostazol inhibited platelet aggregation in a concentration-dependent, non-linear fashion, while ramatroban inhibited linearly with increasing concentration. Anti-platelet effects of drugs having different pharmacological mechanisms were demonstrated clearly by measuring PRP aggregation induced by the three agonists, and by measuring WB aggregation that most probably reflects not only platelet–platelet interactions, but also platelet–leukocyte interactions, as well as the release of intraplatelet molecules. *Blood Coagul Fibrinolysis* **15:157–167 © 2004 Lippincott Williams & Wilkins.**

Blood Coagulation and Fibrinolysis 2004, 15:157–167

Keywords: whole blood aggregation, platelet-rich plasma, aspirin, cilostazol, ramatroban

[a]Department of Clinical Pharmacy and Pharmacology, [b]Department of Thoracic Cardiovascular Surgery, Hepato-Biliary-Pancreatic Surgery, and [c]Department of Oncology, Division of Maxillofacial Radiology and Department of Space Environmental Medicine, Graduate School of Medical and Dental Sciences, Kagoshima University, Kagoshima, Japan.

Sponsorship: This study was supported in part by grant-in-aid for scientific research 13672395 from the Ministry of Education, Culture, Sports, Science and Technology, Japan.

Correspondence and requests for reprints to Kazuo Nakamura, Department of Clinical Pharmacy and Pharmacology, Graduate School of Medical and Dental Sciences, Kagoshima University 8-35-1 Sakuragaoka, Kagoshima 890-8520, Japan.
Tel: +81 99 275 5542; fax: +81 99 265 5293;
e-mail: knaka@denta.hal.kagoshima-u.ac.jp

Received 28 January 2003 **Revised** 26 August 2003
Accepted 4 November 2003

Introduction

Anti-platelet drugs are administered to prevent the formation of thrombus due to platelet activation in patients with myocardial infarction, thrombotic strokes and peripheral vascular disease [1,2]. It is necessary to manage the effects of anti-platelet drugs to within an appropriate therapeutic range to protect patients from the formation of thrombus and bleeding. Measurement of platelet aggregation has been widely carried out to assess platelet function and the effects of anti-platelet drugs. By far the most common method to detect platelet aggregation is by measuring light transmission of platelet-rich plasma (PRP) [3], while another method to detect platelet aggregates in PRP is a light-scattering method based on a particle counting [4,5]. There are also some methods using whole blood (WB) such as electrical impedance aggregometry [6,7], measurement of closure time of an artificial vessel with a bioactive membrane having a microscopic aperture [3,8], light absorbance measurement of blood samples based on agglutination of platelets to fibrinogen-coated beads [3,9,10], and a screen filtration pressure method that measures platelet aggregation in terms of increasing resistance of WB sample flow through a microsieve [11,12]. Notably, the screen filtration pressure method has not been widely utilized to date, largely due to the difficulty of measurement of screen filtration pressure, causing problems with reproducibility and difficulty in the measurement of platelet aggregation. Platelet aggregation is probably mediated by platelet–leukocyte interactions regulated by chemical mediators from leukocytes, erythrocytes and other cells [13,14]. Therefore, it is believed that platelet aggregation in WB could possibly reflect physiological conditions more accurately than aggregation in PRP. Recently, a new type of WB aggregometer with a screen filtration

0957-5235 © 2004 Lippincott Williams & Wilkins

DOI: 10.1097/01.mbc.0000114383.15192.ee

pressure method has been developed; there are some reports regarding this device [15–17].

We have been evaluating *in vitro* anti-platelet effects of the drugs sarpogrelate hydrochloride (a 5-HT_2-serotonergic receptor antagonist) and cilostazol (a phosphodiesterase III inhibitor) [18,19] as well as the clinical usefulness of anti-platelet drugs in patients who underwent mechanical prosthetic valve replacement or arteriosclerosis obliterans [20,21] by measuring PRP aggregability. In our previous reports, anti-platelet drugs inhibited the release of intraplatelet substances such as platelet-derived growth factor [22,23] and transforming growth factor-beta 1 (TGF-β1) [24], which are both contained in the α-granules in resting platelets, and serotonin accompanied with aggregation [18,19].

In the present study, we evaluated the anti-platelet effects of aspirin, cilostazol and ramatroban, a specific thromboxane A_2 (TXA_2) receptor antagonist, on platelet aggregation by measuring both PRP aggregation using the turbidimetric method and WB aggregation using the newly developed screen filtration pressure method, and examined the accuracy of this device by comparing results with PRP aggregation data. We also investigated the release of P-selectin, a platelet α-granule membrane protein [25–27], and TGF-β1 and the formation of TXA_2 in response to platelet agonists as means to evaluate the anti-platelet effects of drugs. Furthermore, detection of platelet–leukocyte interaction in WB aggregometry was examined.

Materials and methods

Reagents

Adenosine diphosphate (ADP) (Sigma, St Louis, Missouri, USA), collagen (General Reagent Collagen Horse Tendon, Hormon-Chemie Co., Ltd., Munich, Germany) and arachidonic acid (Nacalai Tesque, Kyoto, Japan) were used as platelet agonists. Final concentrations of the respective agonists were as follows: ADP, 1, 2, 4, 5 and 8 μmol/l; collagen, 1 μg/ml; and arachidonic acid, 3 mmol/l, as previously described [27,28]. Aspirin was purchased from Sigma. Cilostazol and ramatroban were kindly supplied by Otsuka Pharmaceutical Co., Ltd (Tokushima, Japan) and Bayer AG (Wuppertal, Germany), respectively. Aspirin and ramatroban were dissolved in ethanol and then diluted with saline. Cilostazol was dissolved in *N,N*-dimethylformamide (Nacalai Tesque). Fluorescein isothiocyanate (FITC)-conjugated monoclonal antibody, anti-CD45 and phycoerythrin (PE)-conjugated monoclonal antibody, anti-CD42b, were purchased from Becton Dickinson Pharmingen (San Jose, California, USA).

Preparation of blood sample

Blood samples were collected from healthy volunteers into plastic syringes containing 3.8% sodium citrate (1 : 9). An automatic blood cell counter (Sysmex K-2000; Sysmex, Kobe, Japan) was used to count platelets. In eight healthy volunteers, the mean value of platelet count in WB was $(25.0 \pm 5.0) \times 10^4$ cells/μl. PRP (3×10^5 platelets/μl) and platelet-poor plasma were prepared as previously reported [27,28]. Aliquots of WB and PRP were mixed with a working solution of aspirin and ramatroban (19 : 1), or mixed with a working solution of cilostazol (1 : 399), and then incubated for 3 min at room temperature (23–26°C). Control WB and PRP were mixed with vehicle and incubated similarly. Thus, the final concentrations of ethanol and *N,N*-dimethylformamide were 0.025 and 0.05%, respectively. All subjects were given an explanation of the purpose and design of the study, and consented to donate blood.

Estimation of drug effects on PRP aggregation

PRP obtained 60 min after blood collection was incubated with aspirin, cilostazol or ramatroban at room temperature for 3 min, and then stimulated by ADP (1, 2, 4, 5 and 8 μmol/l), collagen (1 μg/ml) and arachidonic acid (3 mmol/l). PRP aggregation was measured with the turbidimetric method [29], using a Hematracer 801 (M.C. Medical, Tokyo, Japan), and quantified by light transmission as previously reported [27,28]. Effects of drugs on PRP aggregation were estimated by percent maximum aggregation (MA).

Determination of soluble P-selectin, TGF-β1 and thromboxane B_2

PRP samples after measurement of platelet aggregation were centrifuged at $2190 \times g$ for 20 min, and the supernatant was collected to determine the levels of soluble P-selectin (sP-selectin), TGF-β1, and thromboxane B_2 (TXB_2), which is a metabolic product of arachidonic acid and is rapidly formed from TXA_2 but has no biological activity. Samples were stored at −30°C until analysis. The enzyme-linked immunosorbent assay (ELISA) kit for sP-selectin was obtained from Bender MedSystems (Vienna, Austria), the TGF-β1 ELISA kit from R&D Systems, Inc. (Minneapolis, Minnesota, USA) and the TXB_2 ELISA kit from PerSeptive Biosystems (Framingham, Massachusetts, USA).

Measurement of WB aggregation

WB aggregation was measured by a WB aggregometer with the screen filtration pressure method (M.C. Medical). Two hundred microlitres each of WB samples in four reaction tubes was stirred with stirrer bar at 37°C, and pre-incubated for 1 min, followed by the addition of 22 μl each of 1, 2, 4 and 8 μmol/l ADP. Five minutes later, WB samples were sucked to detect aggregation pressure at a rate of 200 μl/6.4 s using a syringe containing screen microsieves made of nickel, 3.7 mm in diameter, with 300 openings of 30×30 μm^2 in a 1-mm-